

copy 35

X68-86017

**NASA TECHNICAL  
MEMORANDUM**

NASA TM SX-1532

NASA TM SX-1532

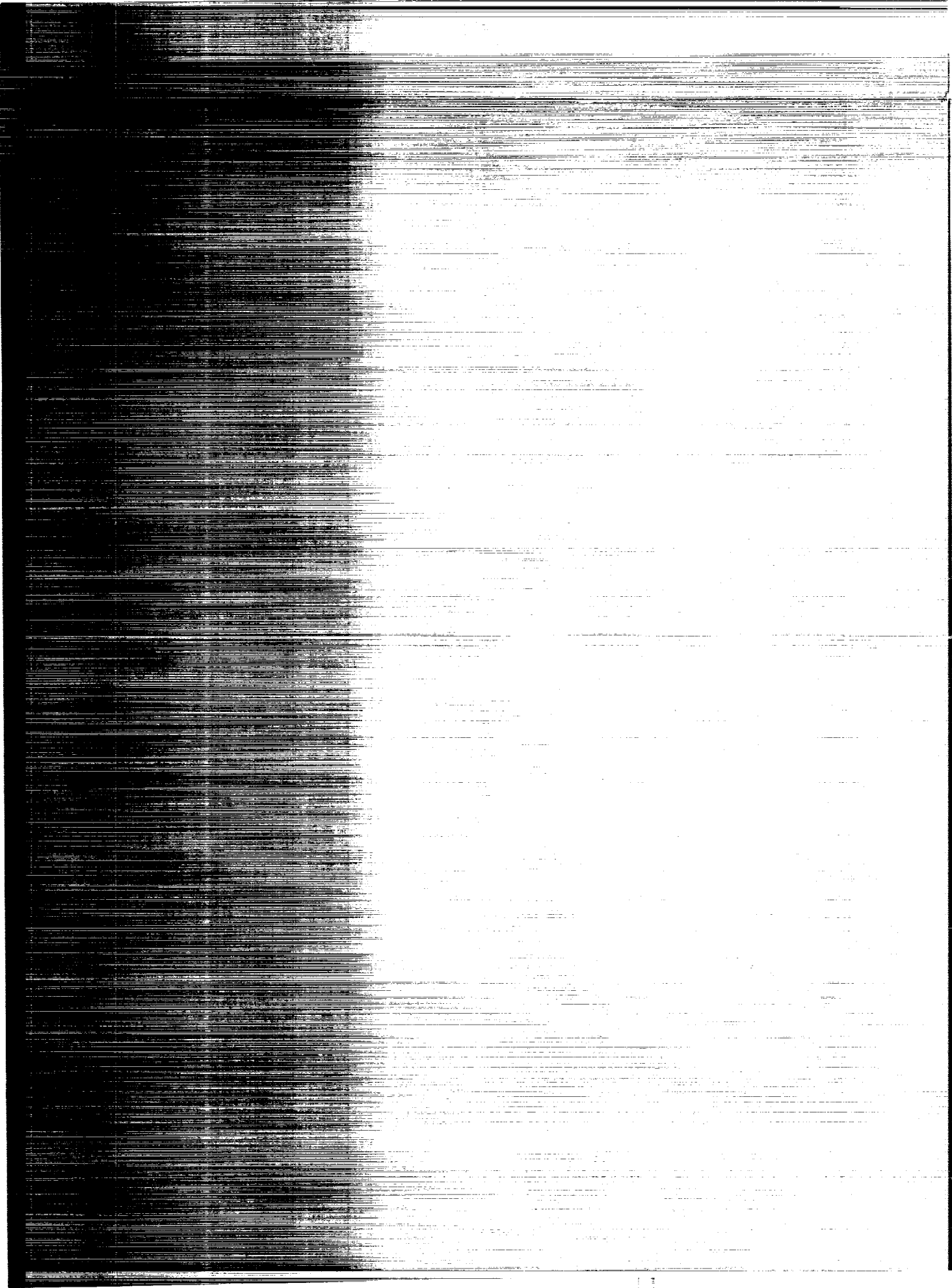
for  
U.S. AIR FORCE

IN-05  
380 492

**AERODYNAMIC CHARACTERISTICS OF A  
REVISED TARGET DRONE VEHICLE AT  
MACH NUMBERS FROM 1.60 TO 2.86**

COORD NO. AF-AM-627

*by A. B. Blair, Jr., and C. Donald Babb*  
*Langley Research Center*  
*Langley Station, Hampton, Va.*



AERODYNAMIC CHARACTERISTICS OF A  
REVISED TARGET DRONE VEHICLE AT  
MACH NUMBERS FROM 1.60 TO 2.86

COORD NO. AF-AM-627

By A. B. Blair, Jr., and C. Donald Babb  
Langley Research Center

ABSTRACT

An investigation has been conducted in the Langley Unitary Plan wind tunnel to determine the aerodynamic characteristics of a revised target drone vehicle through a Mach number range from 1.60 to 2.86. The vehicle had canard surfaces and a swept clipped-delta wing with twin tip-mounted vertical tails.

"STAR Category 01"



TECHNICAL MEMORANDUM SX-1532

for

U.S. Air Force

AERODYNAMIC CHARACTERISTICS OF A  
REVISED TARGET DRONE VEHICLE AT  
MACH NUMBERS FROM 1.60 TO 2.86

COORD NO. AF-AM-627

By A. B. Blair, Jr., and C. Donald Babb

Langley Research Center  
Langley Station, Hampton, Va.

NATIONAL AERONAUTICS AND SPACE ADMINISTRATION

L-5824



AERODYNAMIC CHARACTERISTICS OF A  
REVISED TARGET DRONE VEHICLE AT  
MACH NUMBERS FROM 1.60 TO 2.86

COORD NO. AF-AM-627

By A. B. Blair, Jr., and C. Donald Babb  
Langley Research Center

SUMMARY

An investigation was conducted in the Langley Unitary Plan wind tunnel to determine the static aerodynamic characteristics of a 1/4-scale supersonic target drone vehicle. The model was an outgrowth of an existing target drone and differed primarily by having a longer fuselage. The investigation was made at Mach numbers from 1.60 to 2.86 throughout an angle-of-attack range from about  $-4^{\circ}$  to  $20^{\circ}$ .

The model was longitudinally stable about the center-of-gravity location used in the investigation. The canard surfaces were effective trim devices throughout the Mach number range; although, at high canard settings and angles of attack, canard stall was evident. The model was laterally and directionally stable throughout the angle-of-attack and Mach number ranges. The ailerons were effective in producing rolling moment throughout angle-of-attack range at Mach numbers of 1.60 and 2.86. Generally, positive canard deflection led to increased effective dihedral and negative canard deflection led to decreased effective dihedral. There were significant effects of canard deflection on the directional stability of the model that were dependent on angle of attack and Mach number.

INTRODUCTION

The continuing increase in speed and altitude capability of fighter aircraft has led to the necessity of periodically updating target drone vehicles. As part of a program to develop an expendable supersonic target drone, the Langley Research Center has conducted a wind-tunnel investigation to determine the supersonic aerodynamic characteristics of a 1/4-scale target drone vehicle. The vehicle is air launched, and except for programmed climb-to-cruise altitude, is designed primarily for straight and level flight at Mach numbers up to 3.00 and altitudes to 80 000 feet (24 384 meters). The vehicle is rocket powered and has canard surfaces and twin vertical stabilizers. The vehicle is an outgrowth of an existing target drone (ref. 1) and differed primarily by having a longer fuselage.

The investigation was conducted in the Langley Unitary Plan wind tunnel at Mach numbers from 1.60 to 2.86, at angles of attack from about  $-4^\circ$  to  $20^\circ$ , at angles of side-slip from about  $-4^\circ$  to  $6^\circ$ , and at a Reynolds number of  $10.7 \times 10^6$  based on model length. A limited comparison of data for the revised model with that for the original model (ref. 1) is also included.

### SYMBOLS

The forces and moments have been reduced to nondimensional coefficients based on body cross-sectional area and body length. The longitudinal characteristics are referred to the stability-axis system, and the lateral characteristics are referred to the body-axis system. The moment reference point is located 18.365 inches (46.647 centimeters) forward of the model base. The coefficients and symbols are defined as follows:

A cross-sectional area of body, 0.057625 foot<sup>2</sup> (0.00535 meter<sup>2</sup>)

$C_D$  drag coefficient,  $\frac{\text{Drag}}{qA}$

$C_{D,b}$  base-drag force coefficient,  $\frac{\text{Base-drag force}}{qA}$

$C_{D,c}$  chamber-drag force coefficient,  $\frac{\text{Chamber-drag force}}{qA}$

$C_{D,o}$  drag coefficient for zero lift

$C_L$  lift coefficient,  $\frac{\text{Lift}}{qA}$

$C_{L\alpha}$  lift-curve slope at  $\alpha = 0^\circ$  per degree

$C_l$  rolling-moment coefficient,  $\frac{\text{Rolling moment}}{qAl}$

$C_n$  yawing-moment coefficient,  $\frac{\text{Yawing moment}}{qAl}$

$C_Y$  side-force coefficient,  $\frac{\text{Side force}}{qA}$

$C_{l\beta}$	effective-dihedral parameter, $\frac{\Delta C_l}{\Delta\beta}$ , $\beta = 0^\circ, 3^\circ$
$C_{n\beta}$	directional-stability parameter, $\frac{\Delta C_n}{\Delta\beta}$ , $\beta = 0^\circ, 3^\circ$
$C_{Y\beta}$	side-force parameter, $\frac{\Delta C_Y}{\Delta\beta}$ , $\beta = 0^\circ, 3^\circ$
$C_m$	pitching-moment coefficient, $\frac{\text{Pitching moment}}{qAl}$
$C_{mC_L}$	longitudinal-stability parameter at $C_L \approx 0$
$C_{m\delta_c}$	canard effectiveness in pitch, $\frac{\partial C_m}{\partial \delta_c}$ , per degree
L/D	lift-drag ratio
$l$	body length, 42.996 inches (109.210 centimeters)
M	free-stream Mach number
q	free-stream dynamic pressure, pounds/foot <sup>2</sup> (newtons/meter <sup>2</sup> )
$\alpha$	angle of attack of model center line, degrees
$\beta$	angle of sideslip of model center line, degrees
$\delta_a$	deflection of left-hand aileron minus deflection of right-hand aileron, deflection positive when left-aileron trailing edge is down, degrees
$\delta_c$	deflection of both canards, positive when leading edges are up, degrees

Subscript:

max      maximum

Model component designations:

B        body  
C        canards  
T        vertical tails  
W        wing

## APPARATUS AND METHODS

### Tunnel

An investigation was conducted in the low Mach number test section of the Langley Unitary Plan wind tunnel, which is a variable-pressure continuous-flow facility. The test section is approximately 7 feet (2.13 meters) long and 4 feet (1.22 meters) square. The nozzle leading to the test section is of the asymmetric sliding-block type which permits a continuous variation in Mach numbers from about 1.50 to 2.90.

### Model

A dimensional drawing of the 1/4-scale model is presented in figure 1. The fuselage consists of an ogive-nose—cylinder configuration with a truncated-cone afterbody. The wing was a clipped-delta planform with a modified wedge section. The wing had a leading-edge sweep of  $76^\circ$  and a maximum thickness ratio of 1.54 percent. Full-span ailerons were attached to the wing trailing edge. Twin vertical surfaces were mounted at the wing tips. The test model with canards off is shown in figure 2.

### Tests, Measurements, and Corrections

The model was tested at Mach numbers of 1.60, 1.90, 2.36, and 2.86 at a Reynolds number of  $10.7 \times 10^6$ , based on body length. The stagnation temperature was maintained at  $150^\circ \text{ F}$  ( $339^\circ \text{ K}$ ). The angle-of-attack range of the tests was from about  $-4^\circ$  to  $20^\circ$ . The angle-of-sideslip range was from about  $-4^\circ$  to  $6^\circ$ . The stagnation dewpoint was maintained below  $-30^\circ \text{ F}$  ( $238^\circ \text{ K}$ ) in order to avoid any significant condensation effects in the tunnel. All tests were performed with boundary-layer transition strips on the forebody, wing, vertical tails, and canard surfaces. The transition strips, which were 0.0625 inch (0.15875 centimeter) wide, were composed of No. 60 carborundum grains except on the canards where No. 80 carborundum grains were used. The strips were located 0.4 inch (1.016 centimeters) streamwise from all leading-edge surfaces except on the forebody where the strip was located 1.2 inches (3.048 centimeters) aft of the nose.

Aerodynamic forces and moments were measured by means of a six-component, electrical strain-gage balance mounted within the model. Balance-chamber pressure was measured for all test conditions.

Angles of attack and sideslip were corrected for deflection of the sting-balance combination due to aerodynamic loading. The angles of attack were also corrected for tunnel airflow misalignment. The axial-force (and drag) data were adjusted to correspond to free-stream static conditions in the balance chamber. Typical values of the balance-chamber drag correction are presented in figure 3. Also included in figure 3 are base-drag coefficient values; however, these values are not included in the adjustment of the drag of the vehicle.

## RESULTS AND DISCUSSION

### Longitudinal Characteristics

The longitudinal aerodynamic characteristics for various component arrangements of the model are presented in figure 4. The body-alone results indicated an increase in lift-curve slope with increase in angle of attack at all test Mach numbers. This increase was also evident in all other stages of buildup of the model. The body alone was unstable about the selected center-of-gravity location and the addition of canards caused a further decrease in the stability level of the vehicle. Addition of the wing provided a stable condition for the model, and addition of the vertical stabilizers led to a further increase in stability level because of an end-plating effect. The complete configuration was stable throughout the test Mach number range.

The longitudinal control characteristics of the model are presented in figure 5. The canard surfaces were effective trim devices throughout the Mach number range, although, at high canard settings and angles of attack, canard stall was evident.

A summary of the longitudinal aerodynamic characteristics of the complete model is presented in figure 6. Comparative data for the model in reference 1 are also included. The data indicated the usual decrease in drag coefficient at zero lift, canard effectiveness, lift-curve slope, and stability level with increase in Mach number; these trends were also evident for the model in reference 1 up to  $M = 2.10$ . At comparable Mach numbers, the stability level, canard effectiveness, and drag coefficient at zero lift were somewhat greater for the revised model than for the model in reference 1.

### Lateral Characteristics

The effect of angle of attack on the variation of the lateral aerodynamic characteristics for the complete configuration is presented in figure 7. These data are primarily shown to indicate the linearity of the coefficients with sideslip angle because all lateral

parameters were obtained from incremental results of tests made throughout the angle-of-attack range at  $\beta = 0^\circ$  and  $3^\circ$ . The results were generally linear to  $\beta = 3^\circ$  and indicated that the comparative results shown for the lateral parameters are valid.

The variation of the lateral derivatives with angle of attack at all test Mach numbers for various model arrangements is presented in figure 8. These data show that the complete model was directionally stable and exhibited positive effective dihedral throughout the operating angle-of-attack and Mach number ranges. A pronounced effect of the canard flow field on the directional stability was evident throughout the angle-of-attack range.

Figure 9 presents the variation of the lateral derivatives with Mach number for the complete model near  $\alpha = 0^\circ$ . These data show the usual decrease in directional stability and effective dihedral with increasing Mach number. Data for the model in reference 1 are included for comparison with the revised model. No large differences are evident in the derivative data of the revised model compared with that for the model in reference 1.

The effect of aileron deflection on the lateral characteristics of the model is shown in figure 10 for canard deflections of  $0^\circ$ ,  $10^\circ$ , and  $-10^\circ$  at Mach numbers of 1.60 and 2.86. The ailerons were generally effective in producing rolling moment throughout the angle-of-attack range at both test Mach numbers. Except for an aileron deflection of  $10^\circ$  at a canard deflection of  $0^\circ$  at  $M = 1.60$ , the ailerons produced an unfavorable yawing moment at the lower Mach number, little effect being noticed at the higher Mach number. There is no significant effect of aileron deflection on the lateral derivatives of the model at Mach numbers of 1.60 and 2.86 (fig. 11).

The effect of canard deflection on the lateral derivatives of the model is shown in figure 12. Generally, positive canard deflection led to increased effective dihedral and negative canard deflection led to decreased effective dihedral. This effect of canard deflection on  $C_{l\beta}$  was decreased by increases in both angle of attack and Mach number. There were significant effects of canard deflection on the directional stability of the model that were dependent on angle of attack and Mach number. In general, at low angles of attack, positive canard deflection led to increased directional stability and negative canard deflection led to decreased directional stability.

## CONCLUSIONS

An investigation of a 1/4-scale supersonic target drone vehicle was conducted in the Langley Unitary Plan wind tunnel at Mach numbers from 1.60 to 2.86. The results of the investigation indicated the following conclusions:

1. The model is longitudinally stable about the center-of-gravity location used in the investigation. The canard surfaces are effective trim devices throughout the Mach number range; although at high canard settings and angles of attack, canard stall is evident.

2. The model is laterally and directionally stable throughout angle-of-attack and Mach number ranges.

3. The ailerons are generally effective in producing rolling moment throughout angle-of-attack range at Mach numbers of 1.60 and 2.86.

4. Generally, positive canard deflection leads to increased effective dihedral and negative canard deflection leads to decreased effective dihedral. There are significant effects of canard deflection on the directional stability of the model that are dependent on angle of attack and Mach number.

Langley Research Center,  
National Aeronautics and Space Administration,  
Langley Station, Hampton, Va., November 27, 1967,  
126-13-02-31-23.

#### REFERENCE

1. Blair, A. B., Jr.; and Fournier, Roger H.: Aerodynamic Characteristics of a Target Drone Vehicle at Mach Numbers From 1.57 to 2.10 - COORD No. AF-AM-627. NASA TM SX-1531, U.S. Air Force, 1968.

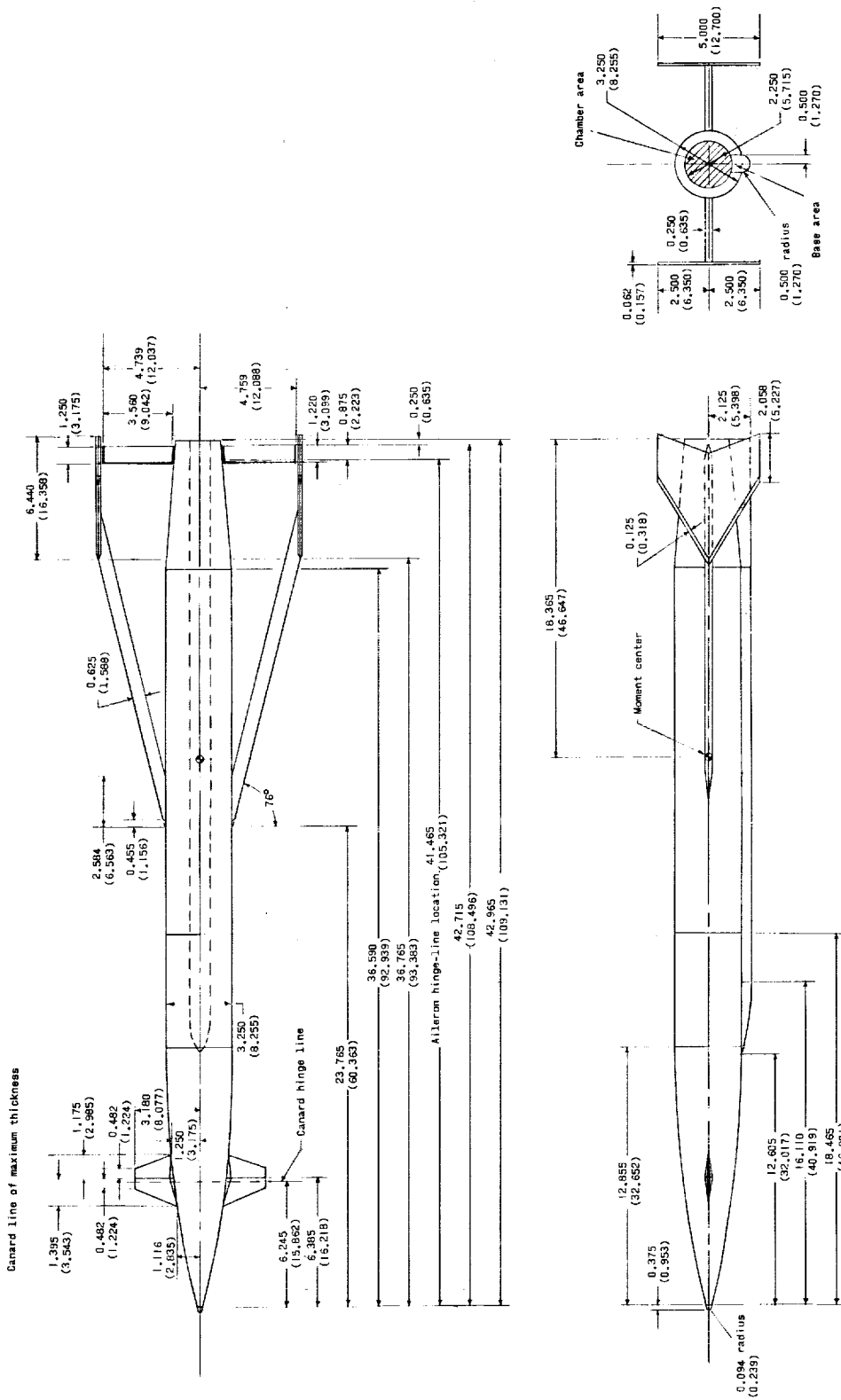


Figure 1.- Dimensional details of the 1/4-scale model used in the investigation. All dimensions are given in inches and parenthetically in centimeters.



Figure 2.- Test model. Canards off.

L-66-7288

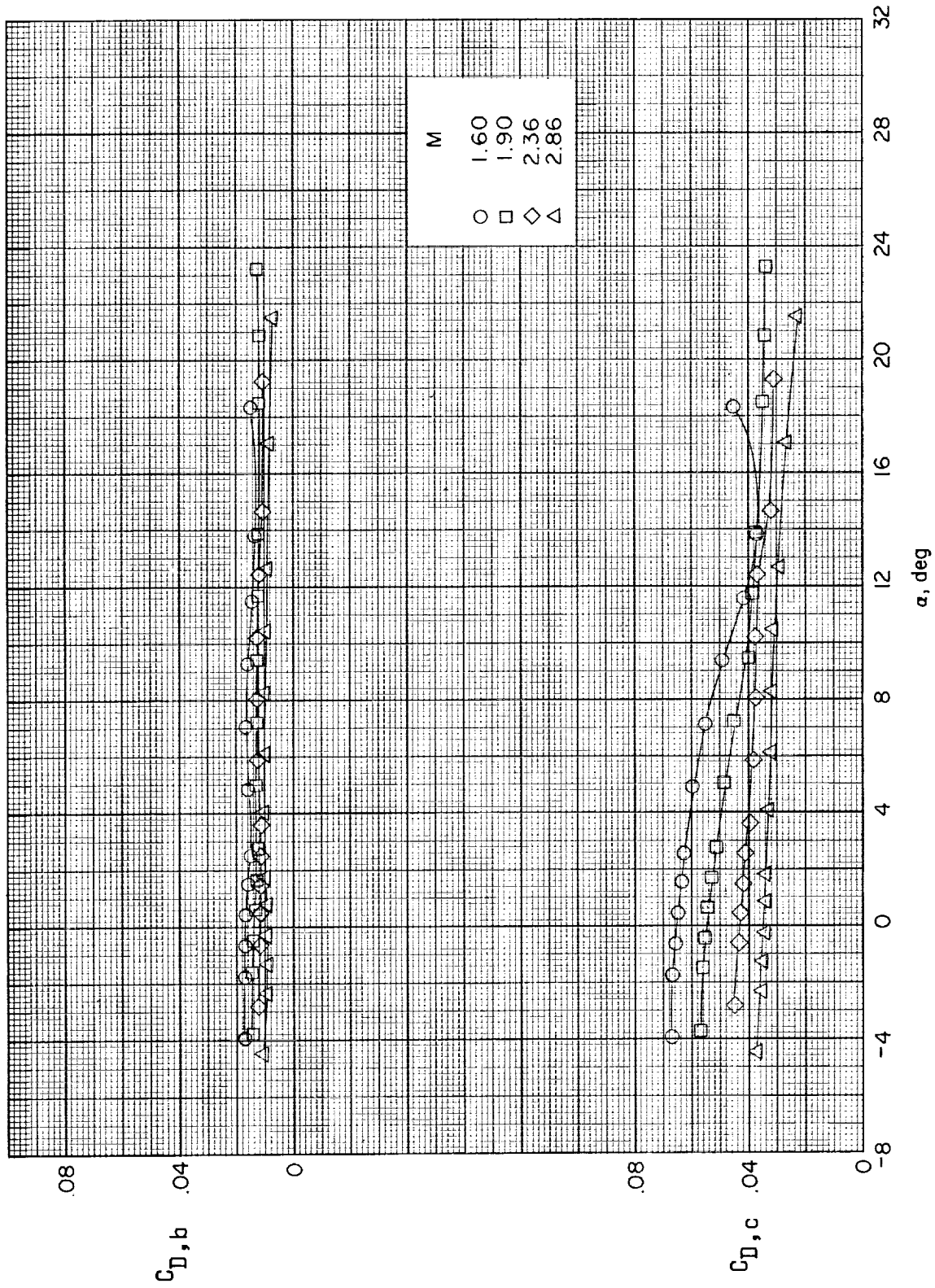
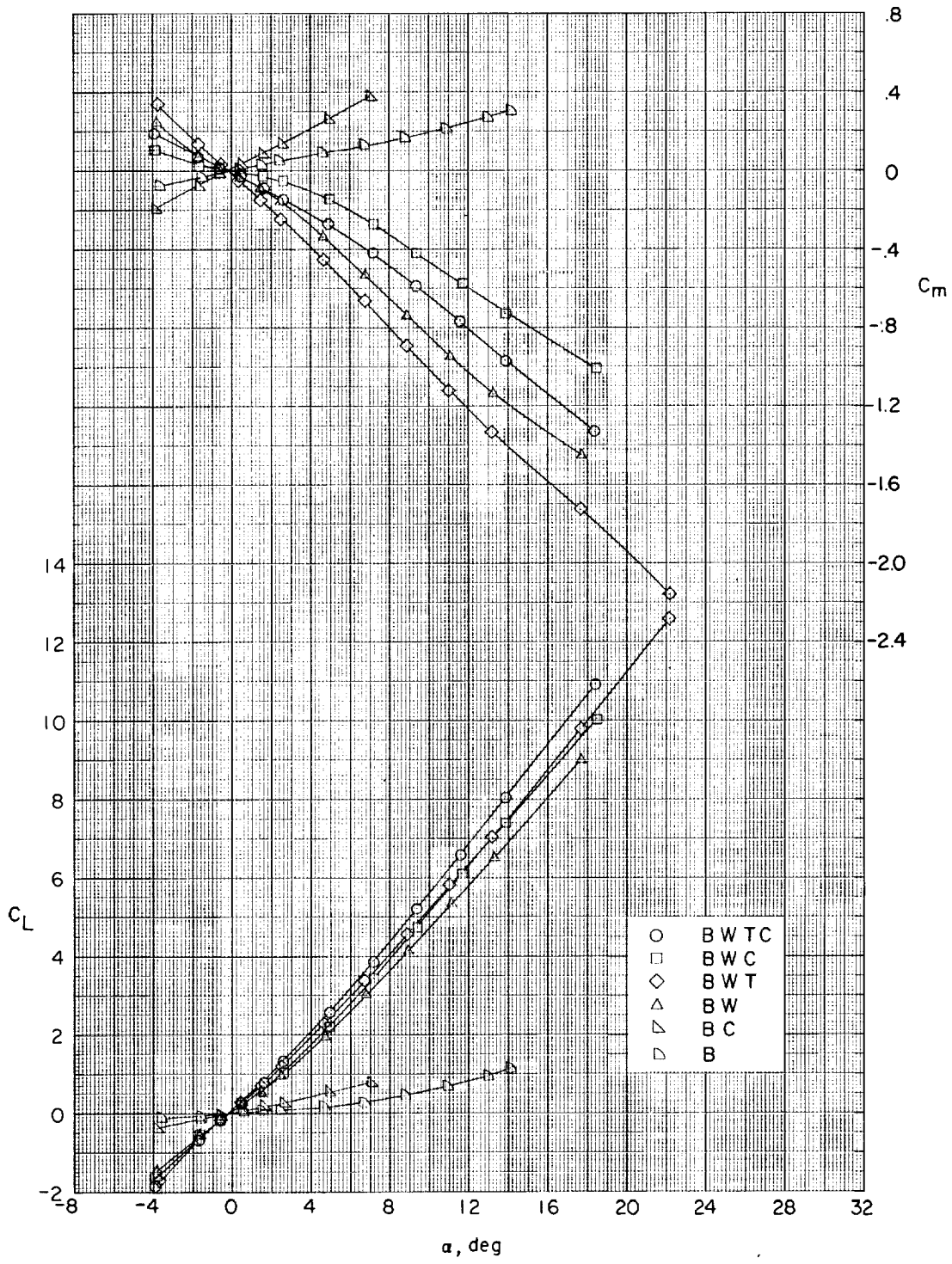
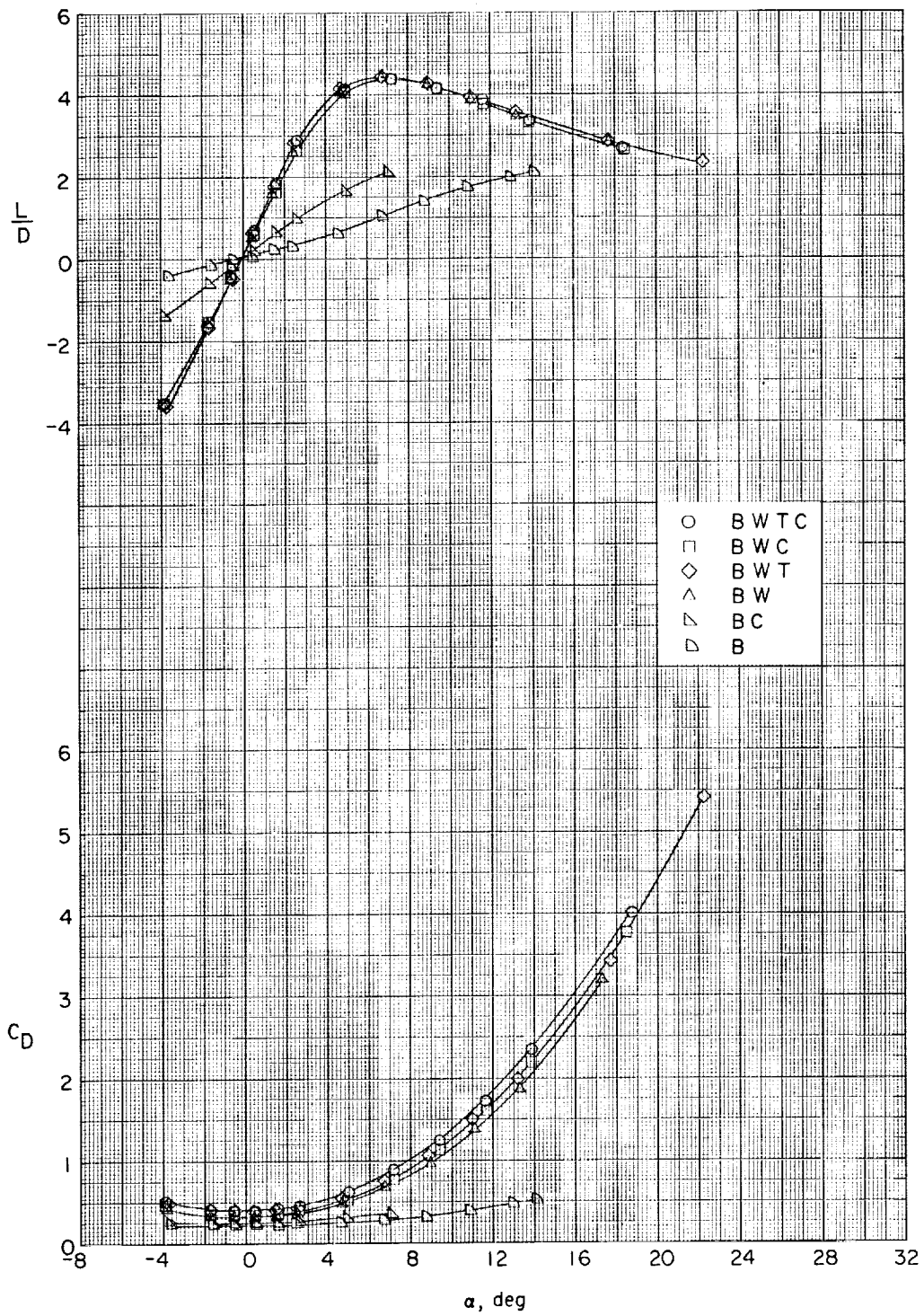


Figure 3.- Typical values of balance-chamber and base-drag coefficients of BWTC.



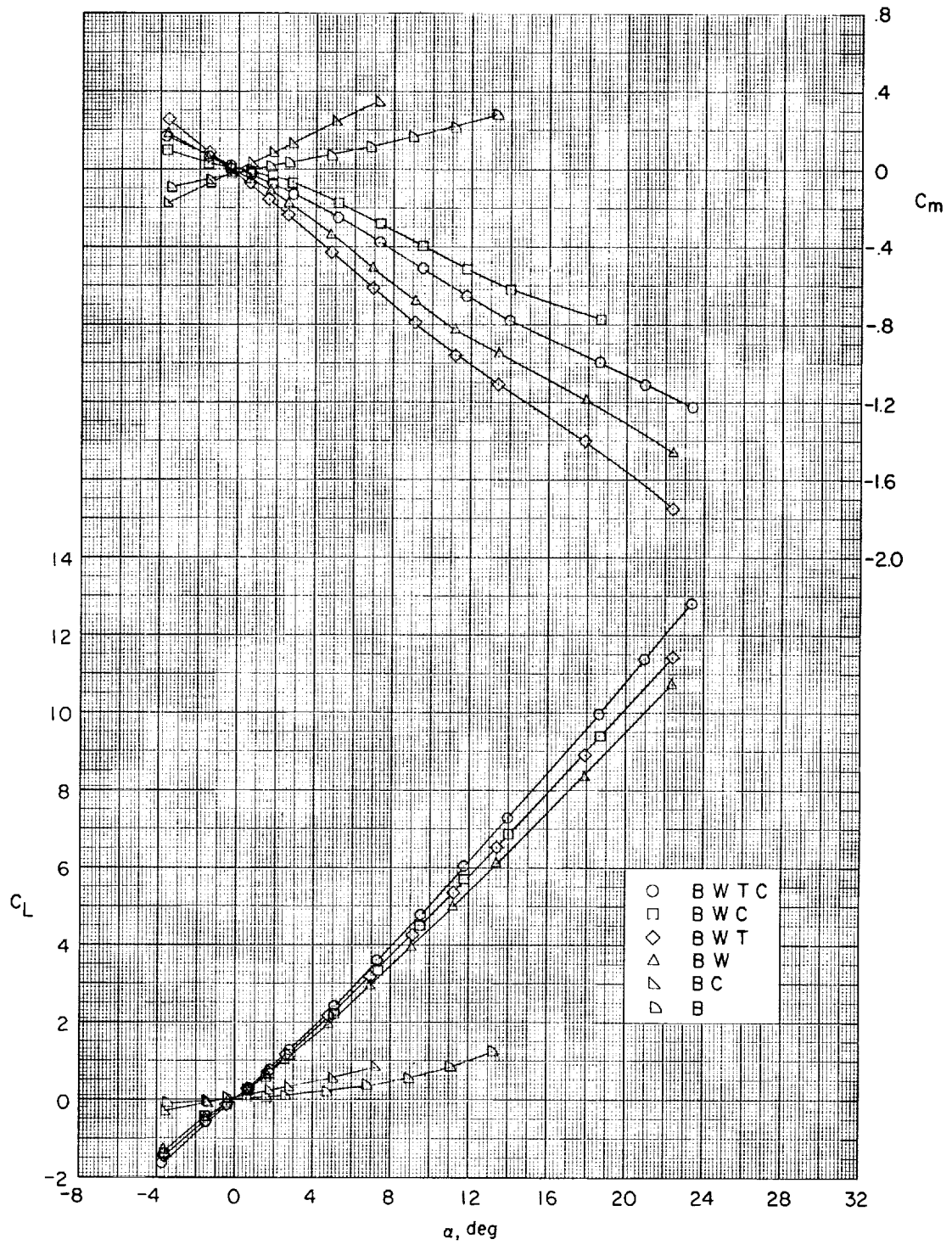
(a)  $M = 1.60$ .

Figure 4.- Longitudinal characteristics for various model arrangements.



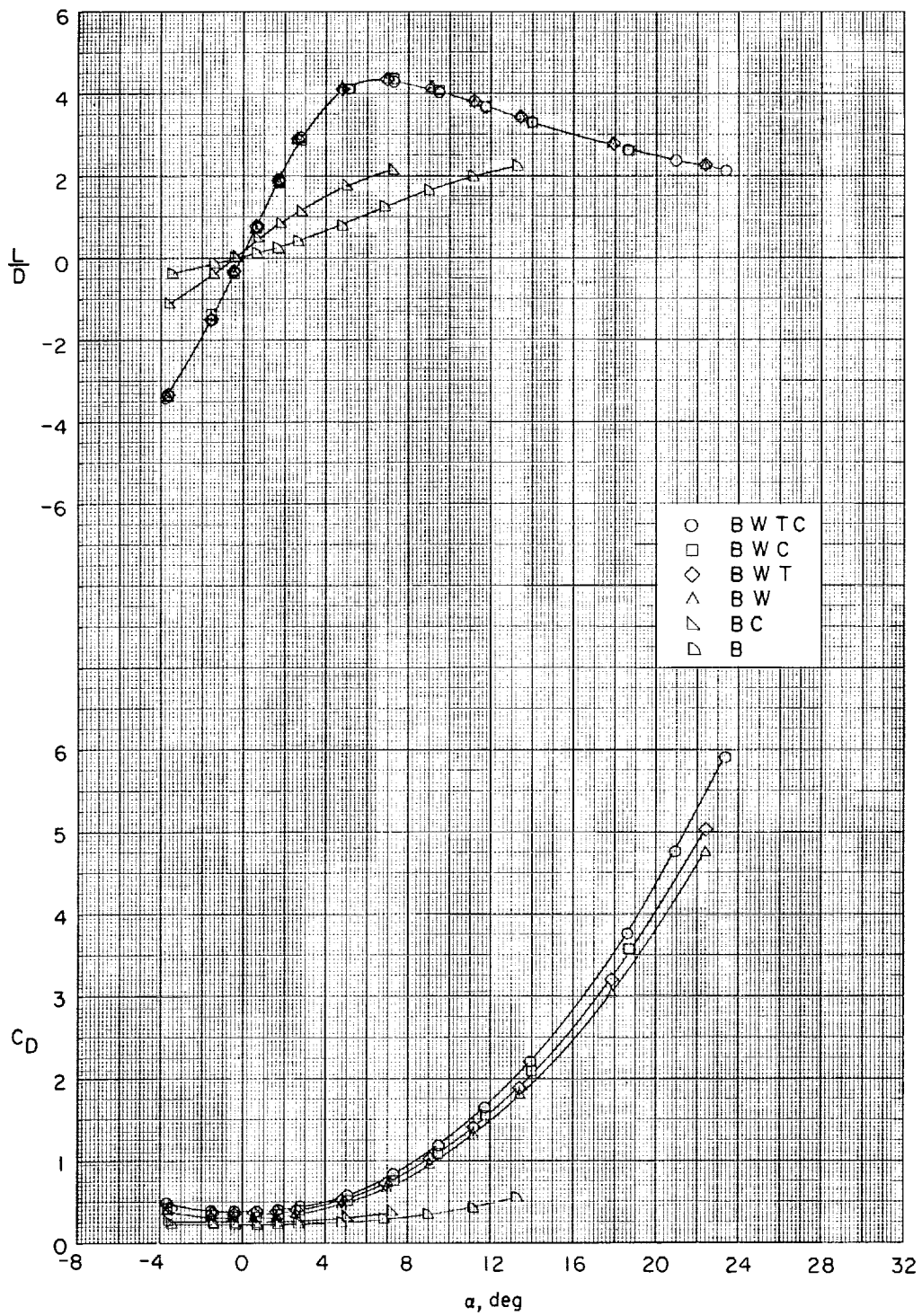
(a) Concluded.

Figure 4.- Continued.



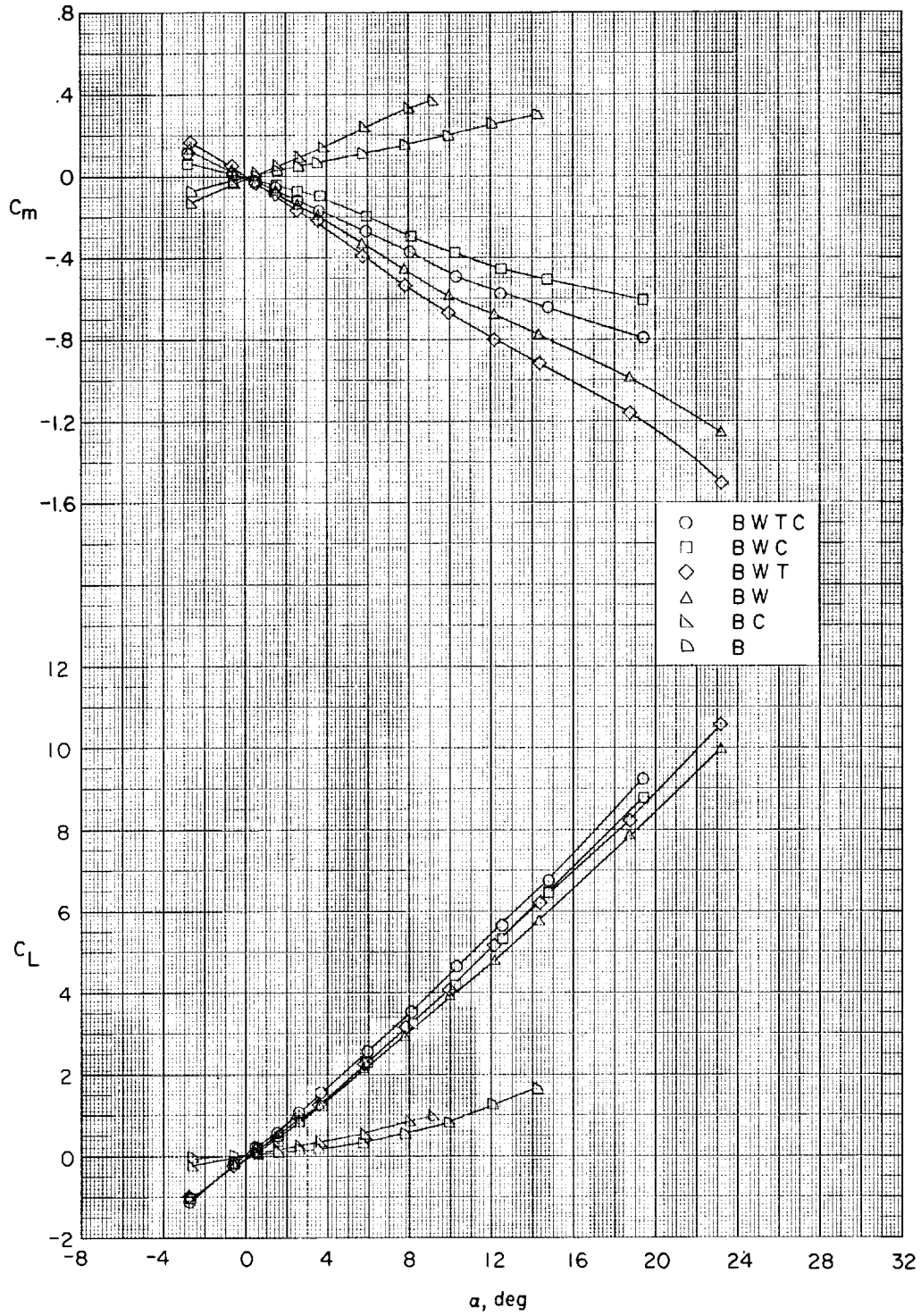
(b)  $M = 1.90$ .

Figure 4.- Continued.



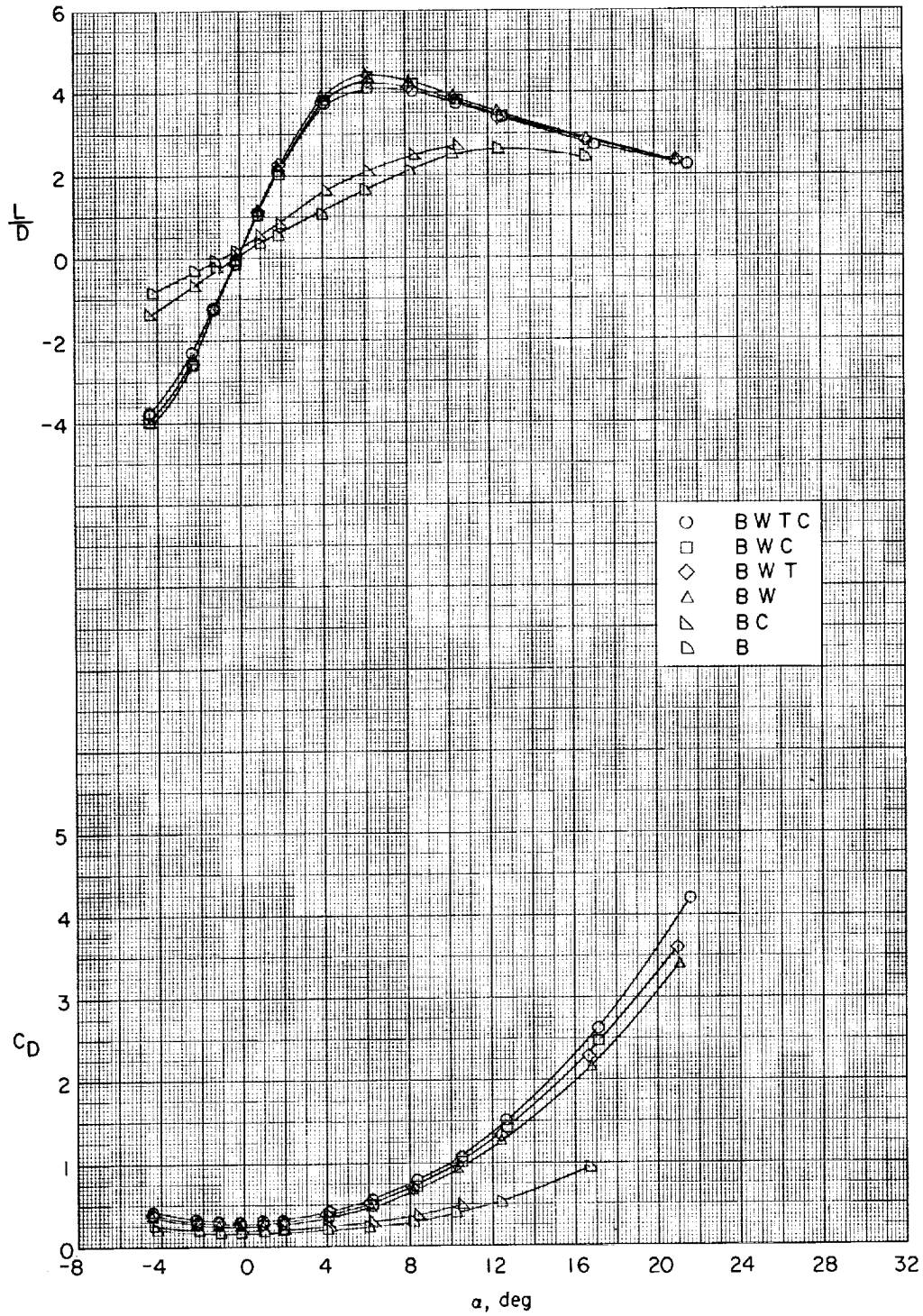
(b) Concluded.

Figure 4.- Continued.



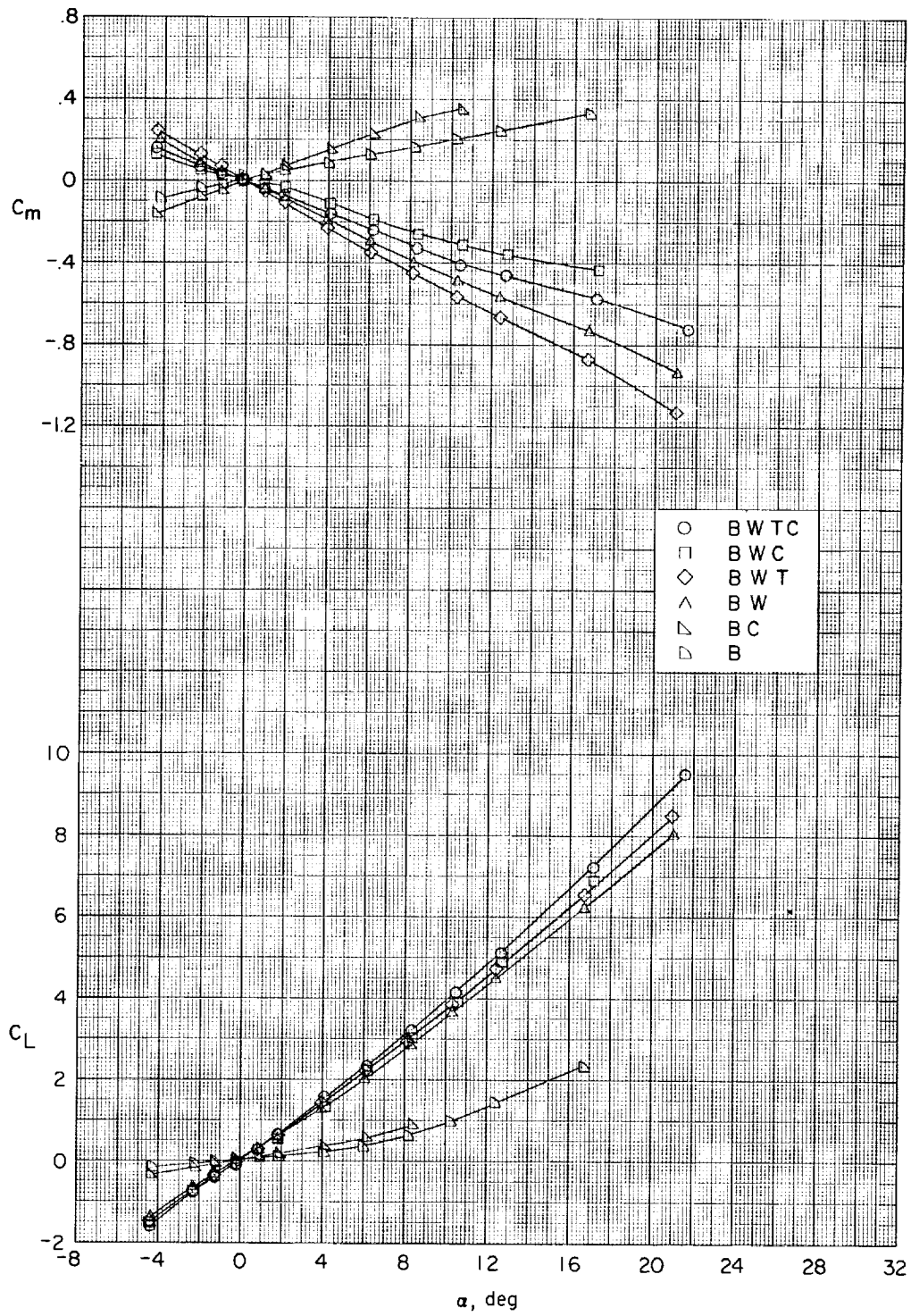
(c)  $M = 2.36$ .

Figure 4.- Continued.



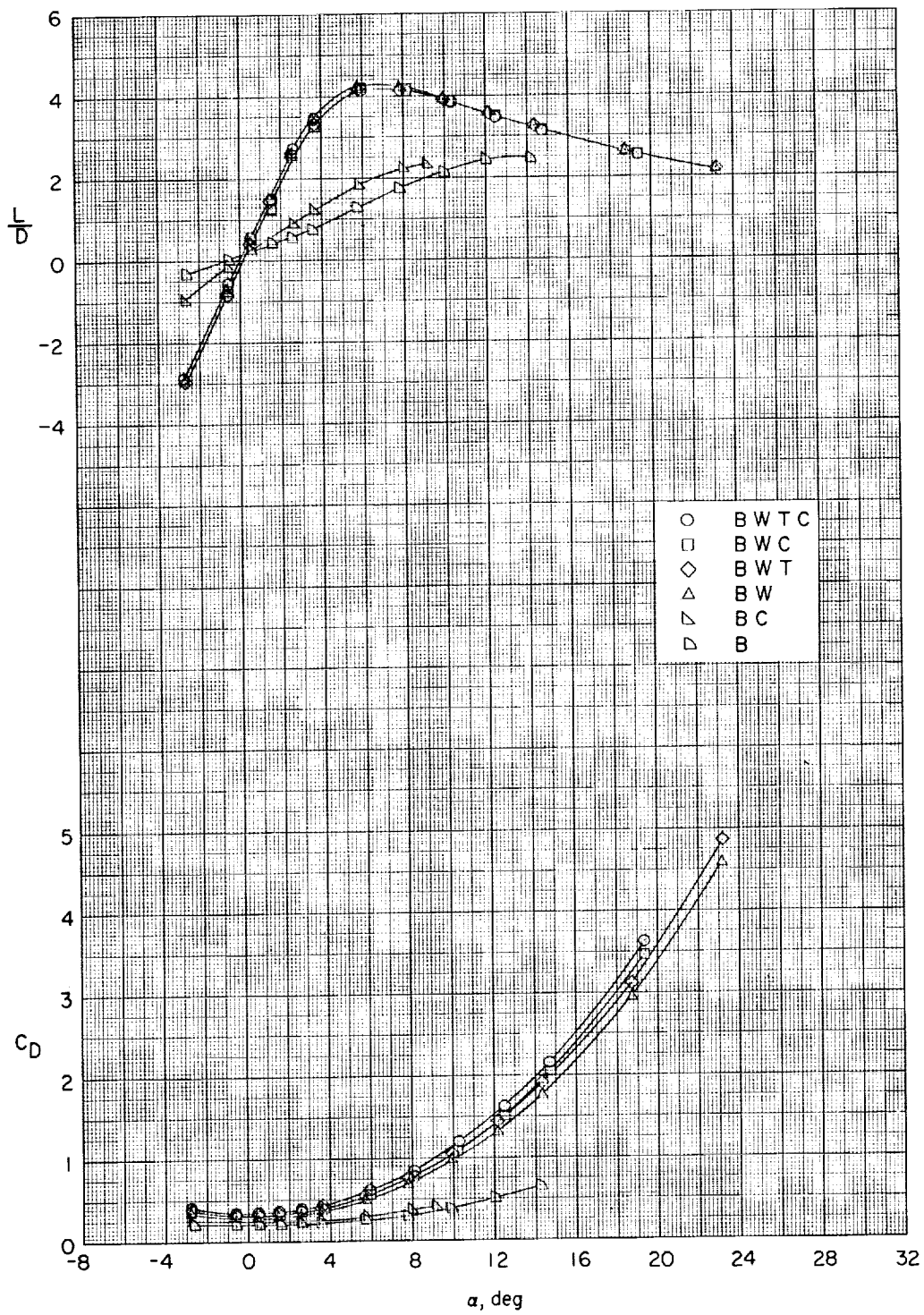
(c) Concluded.

Figure 4.- Continued.



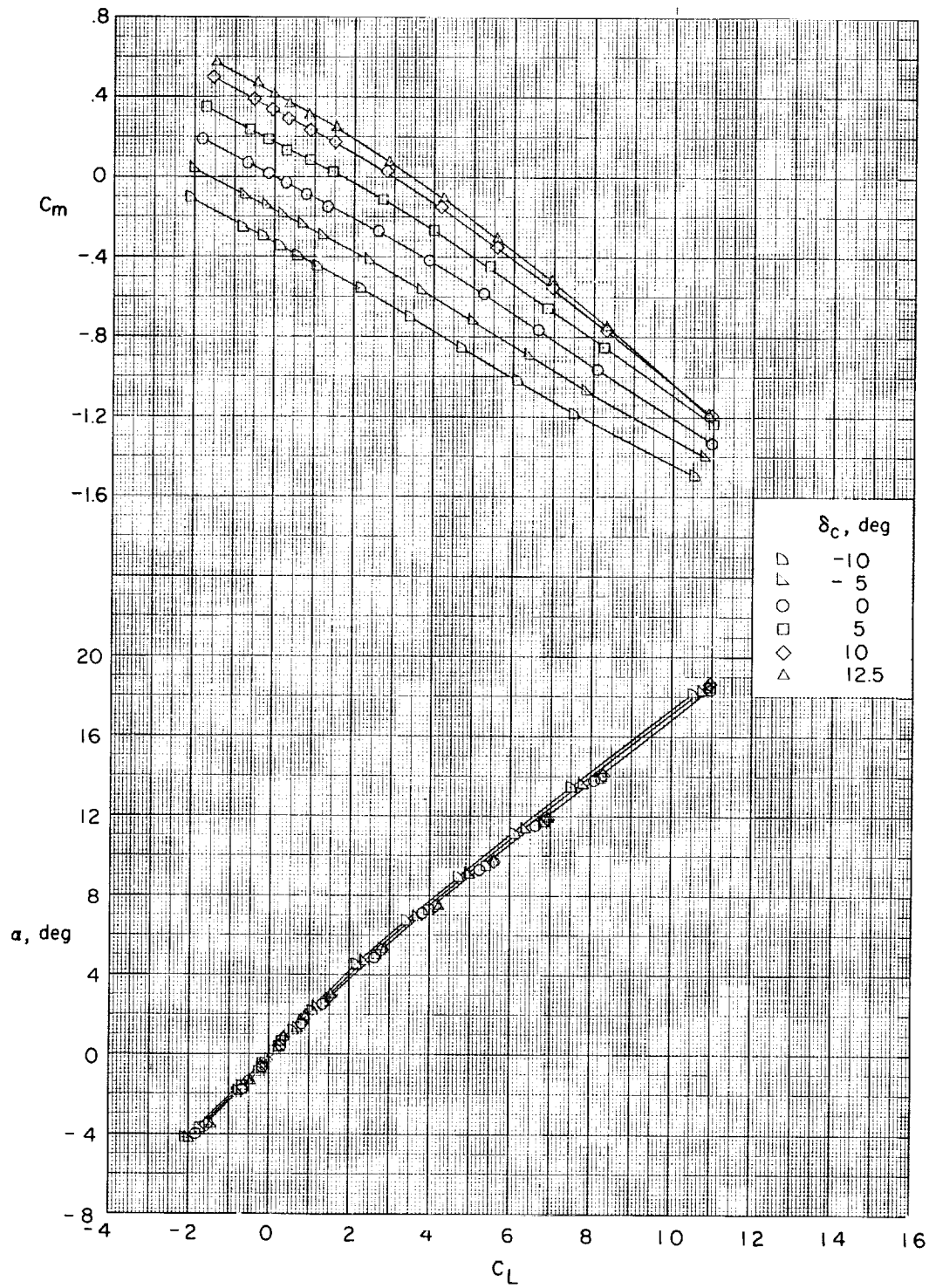
(d)  $M = 2.86$ .

Figure 4.- Continued.



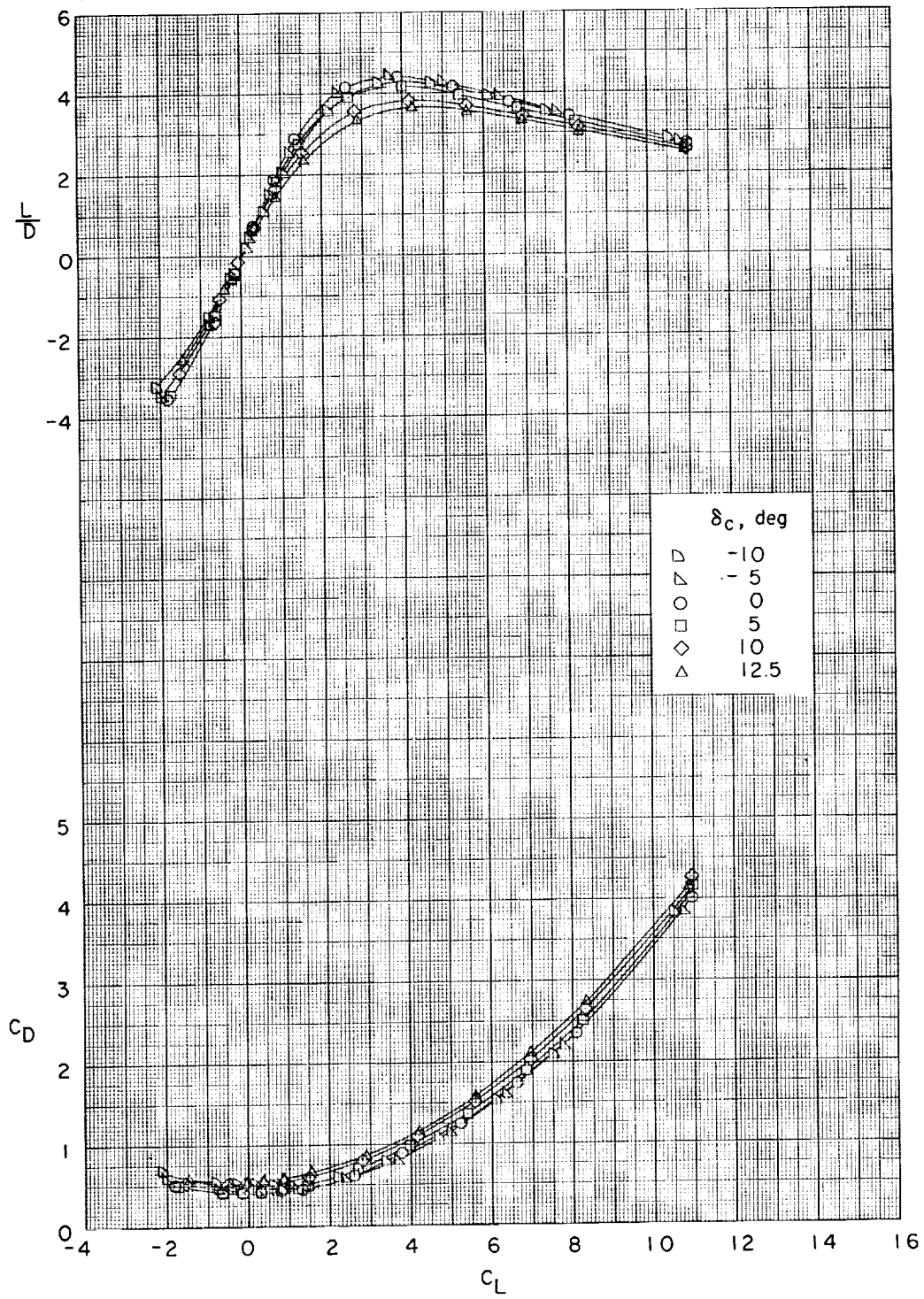
(d) Concluded.

Figure 4.- Concluded.



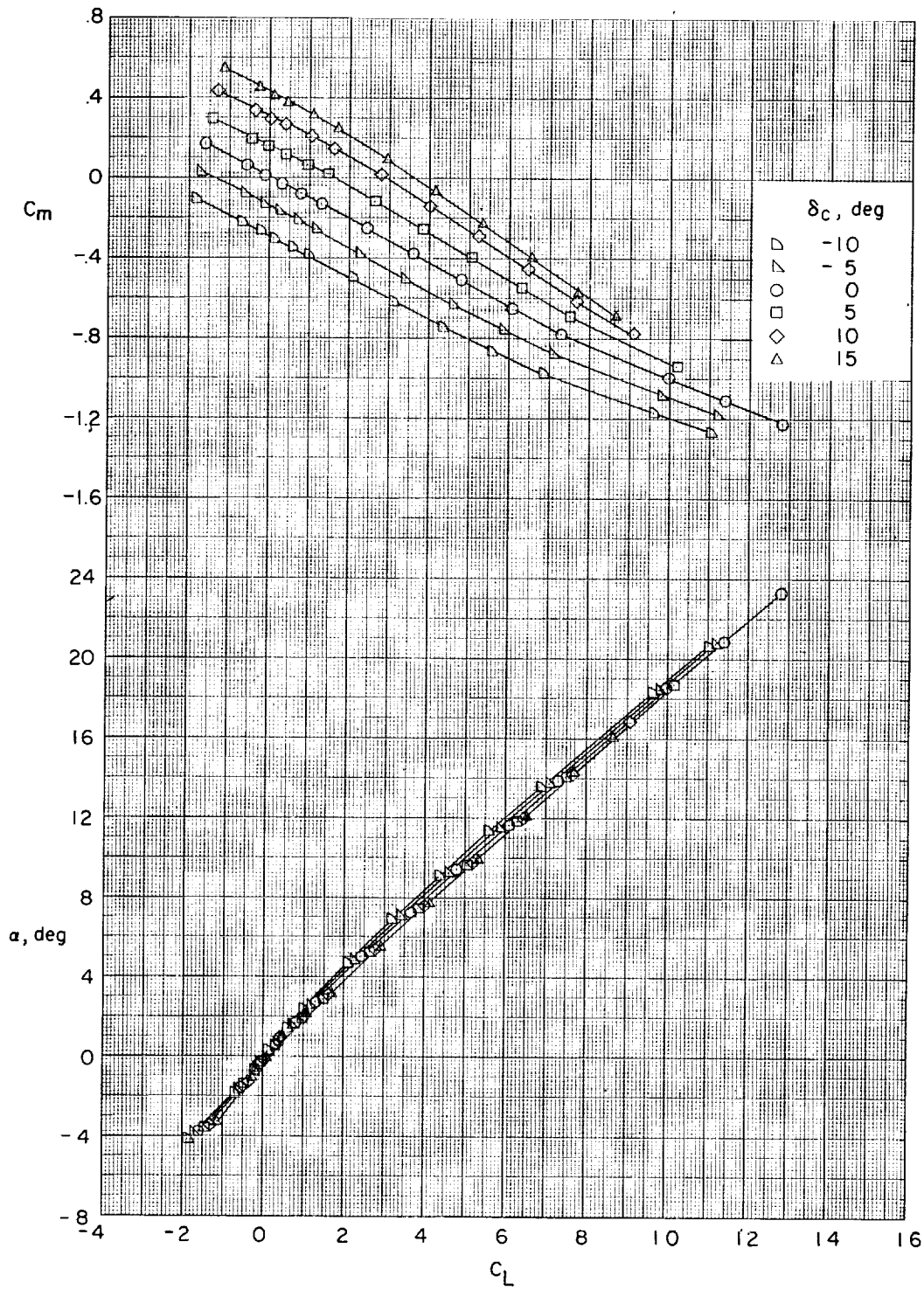
(a)  $M = 1.60$ .

Figure 5.- Longitudinal control characteristics of BWTC.



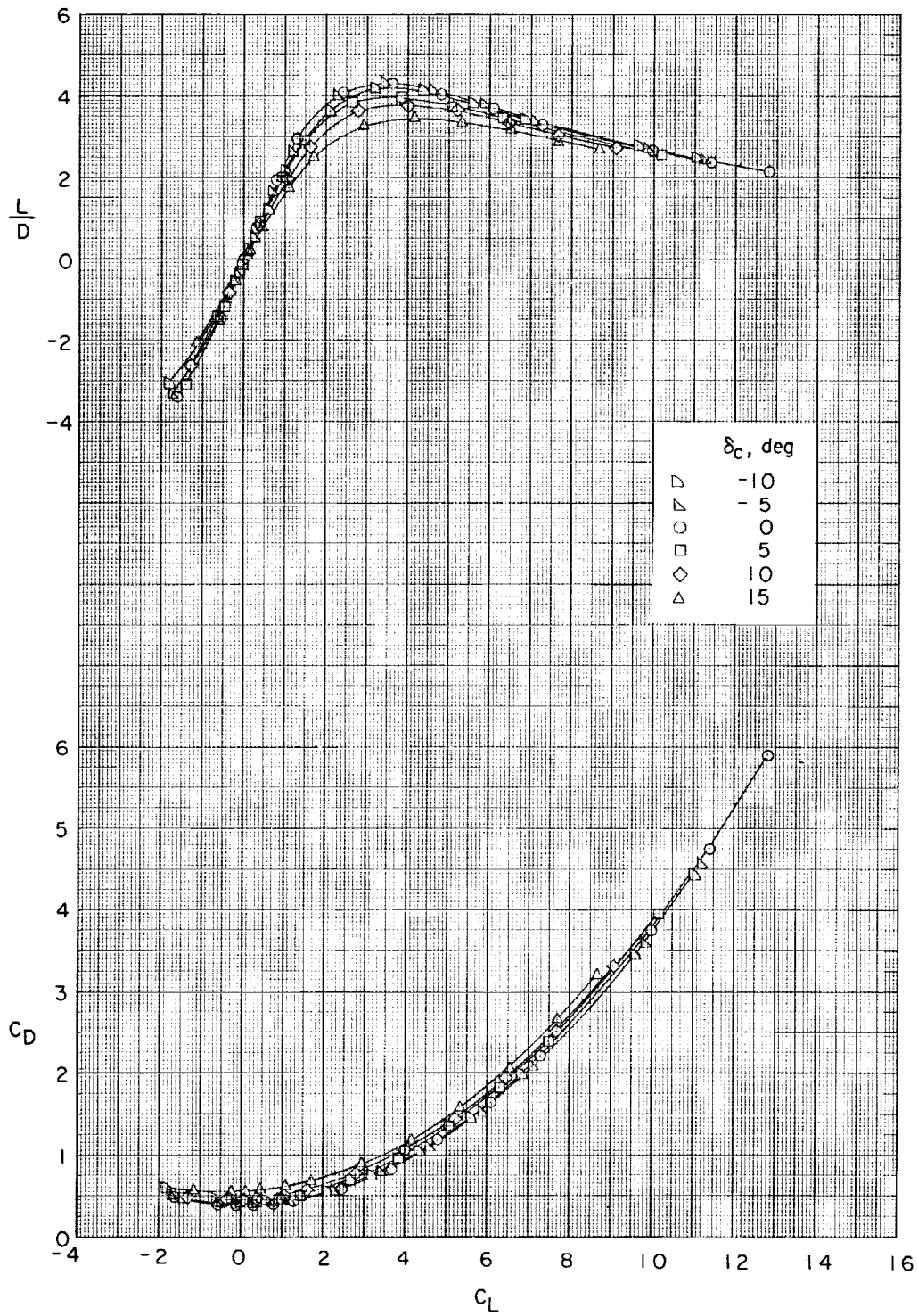
(a) Concluded.

Figure 5.- Continued.



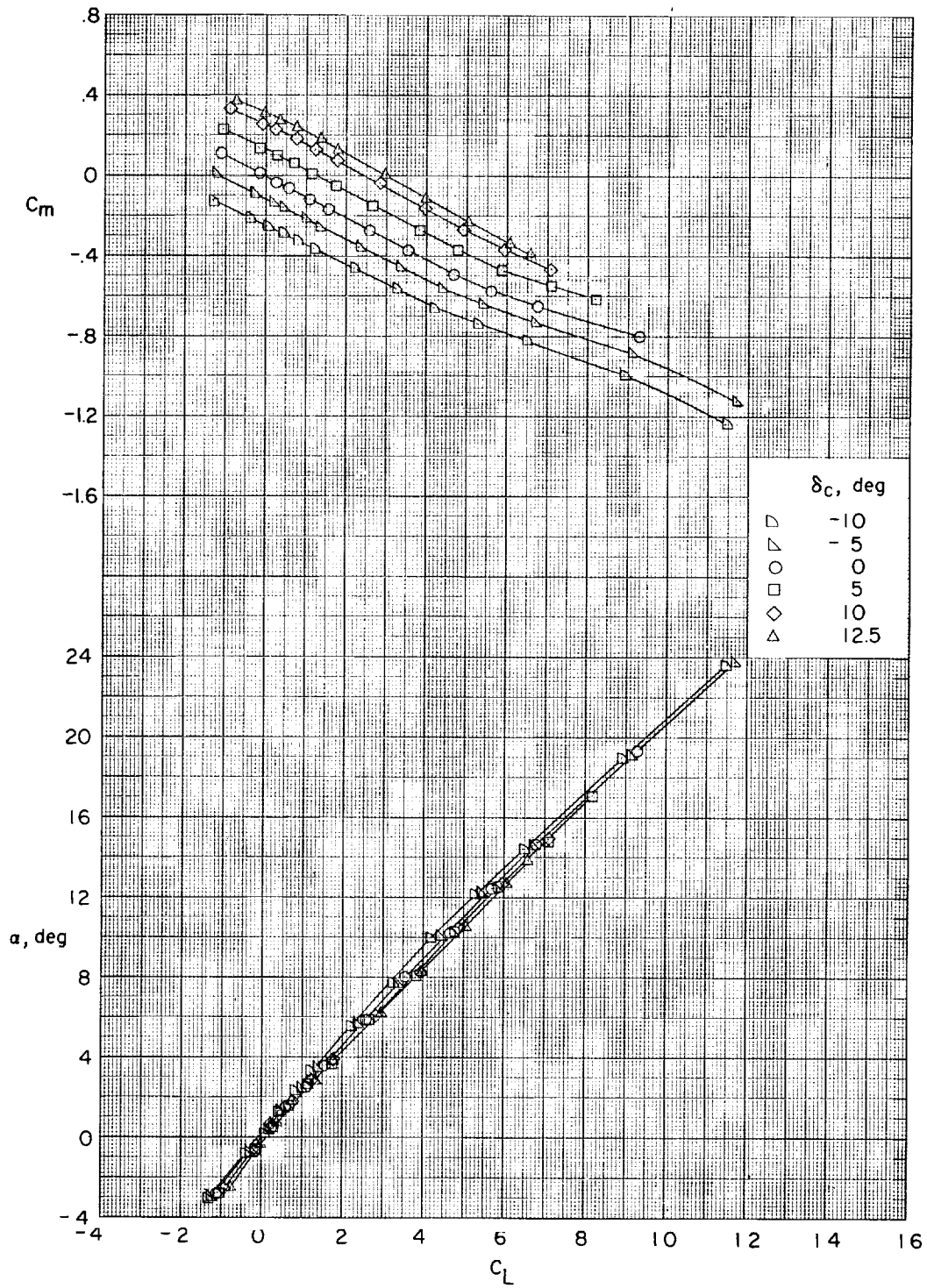
(b)  $M = 1.90$ .

Figure 5.- Continued.



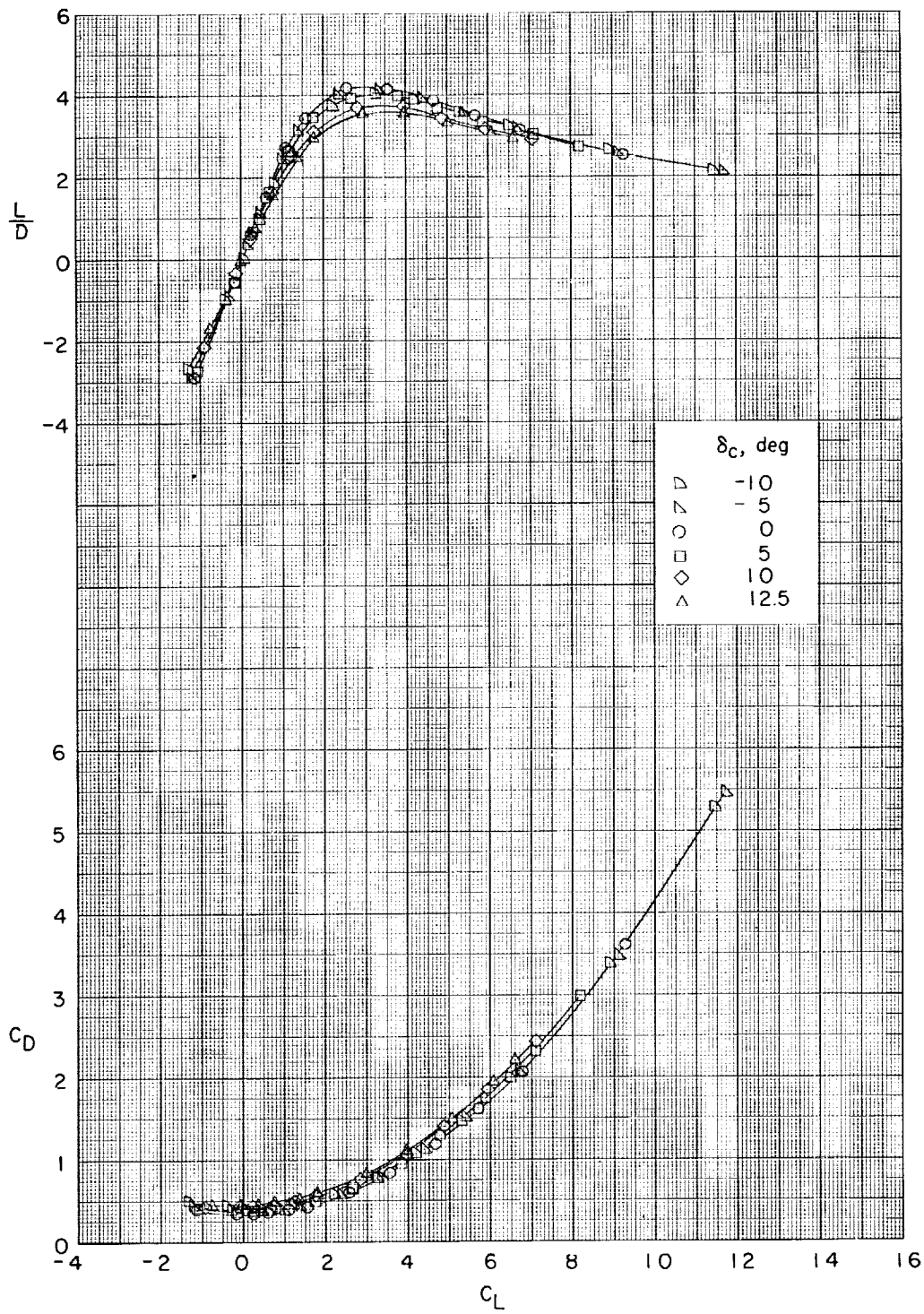
(b) Concluded.

Figure 5.- Continued.



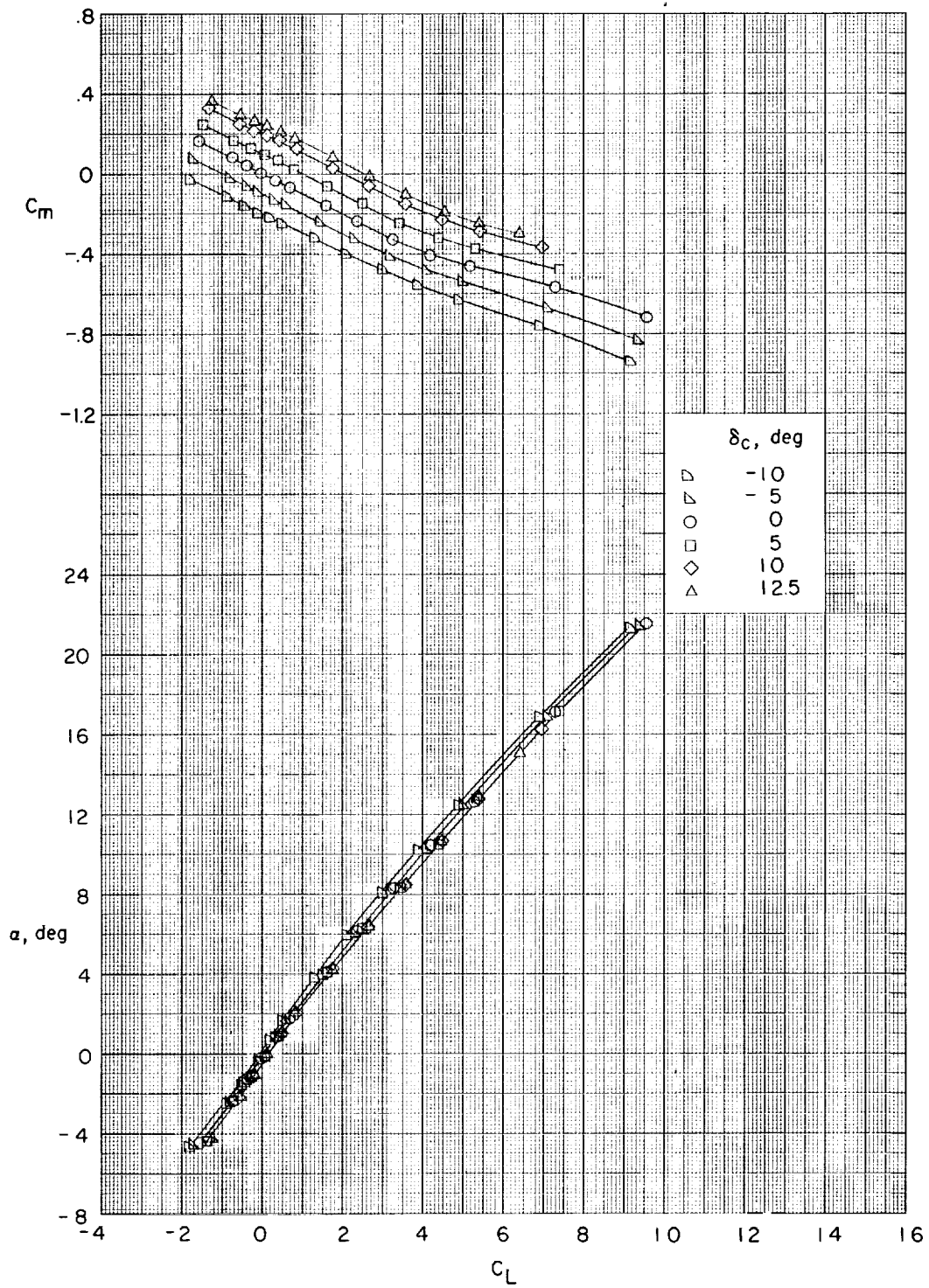
(c)  $M = 2.36$ .

Figure 5.- Continued.



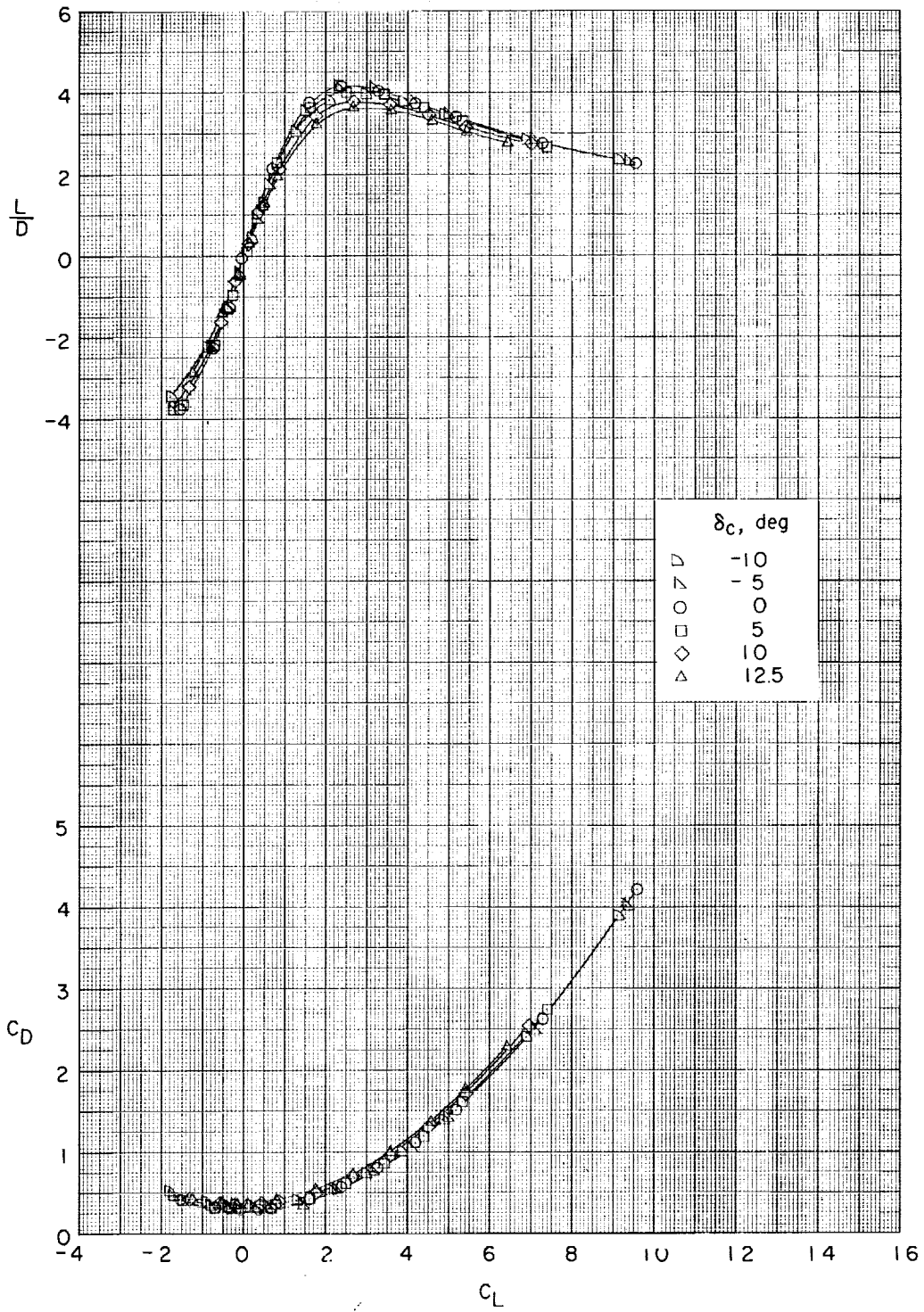
(c) Concluded.

Figure 5.- Continued.



(d)  $M = 2.86$ .

Figure 5.- Continued.



(d) Concluded.

Figure 5.- Concluded.

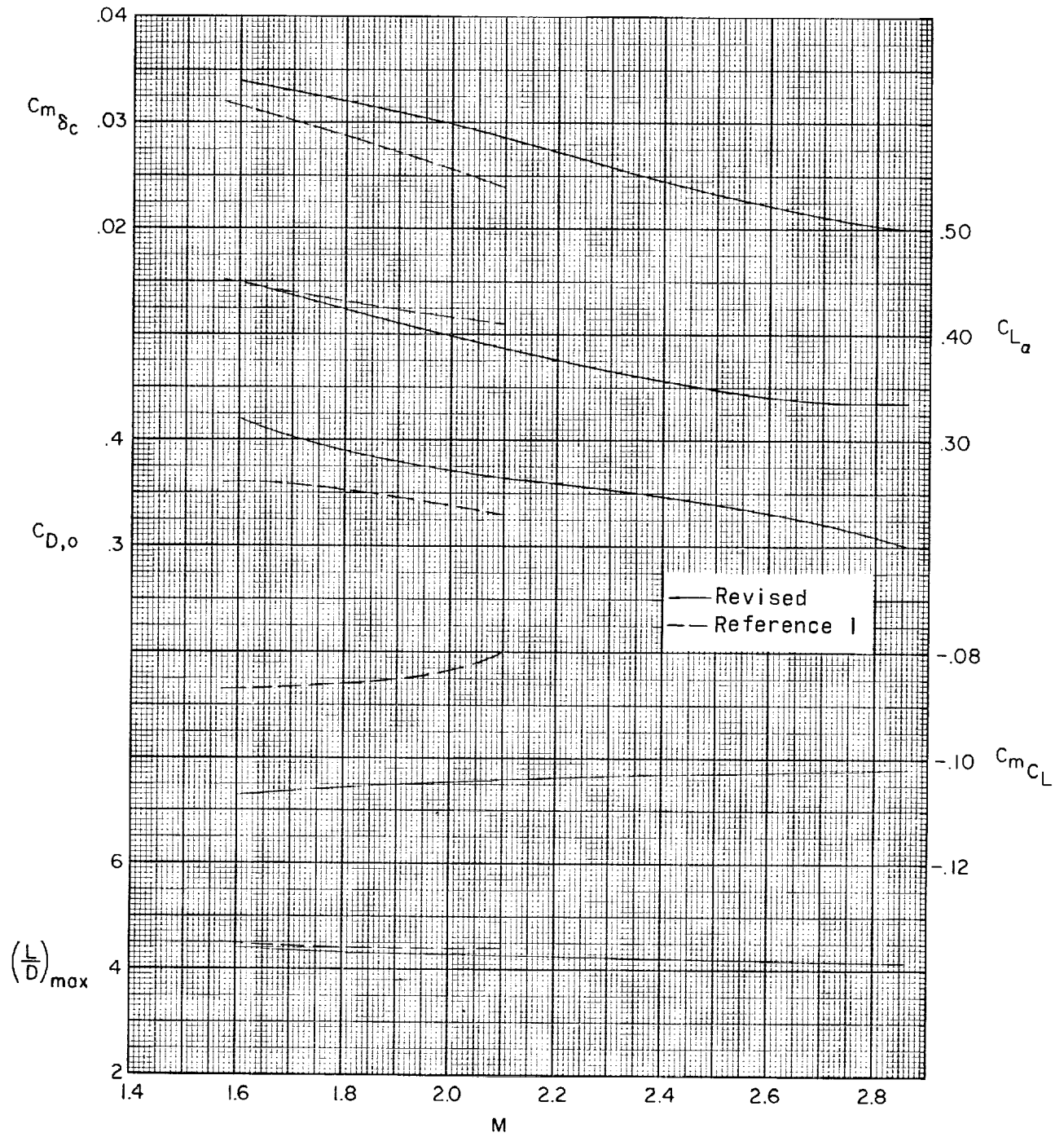
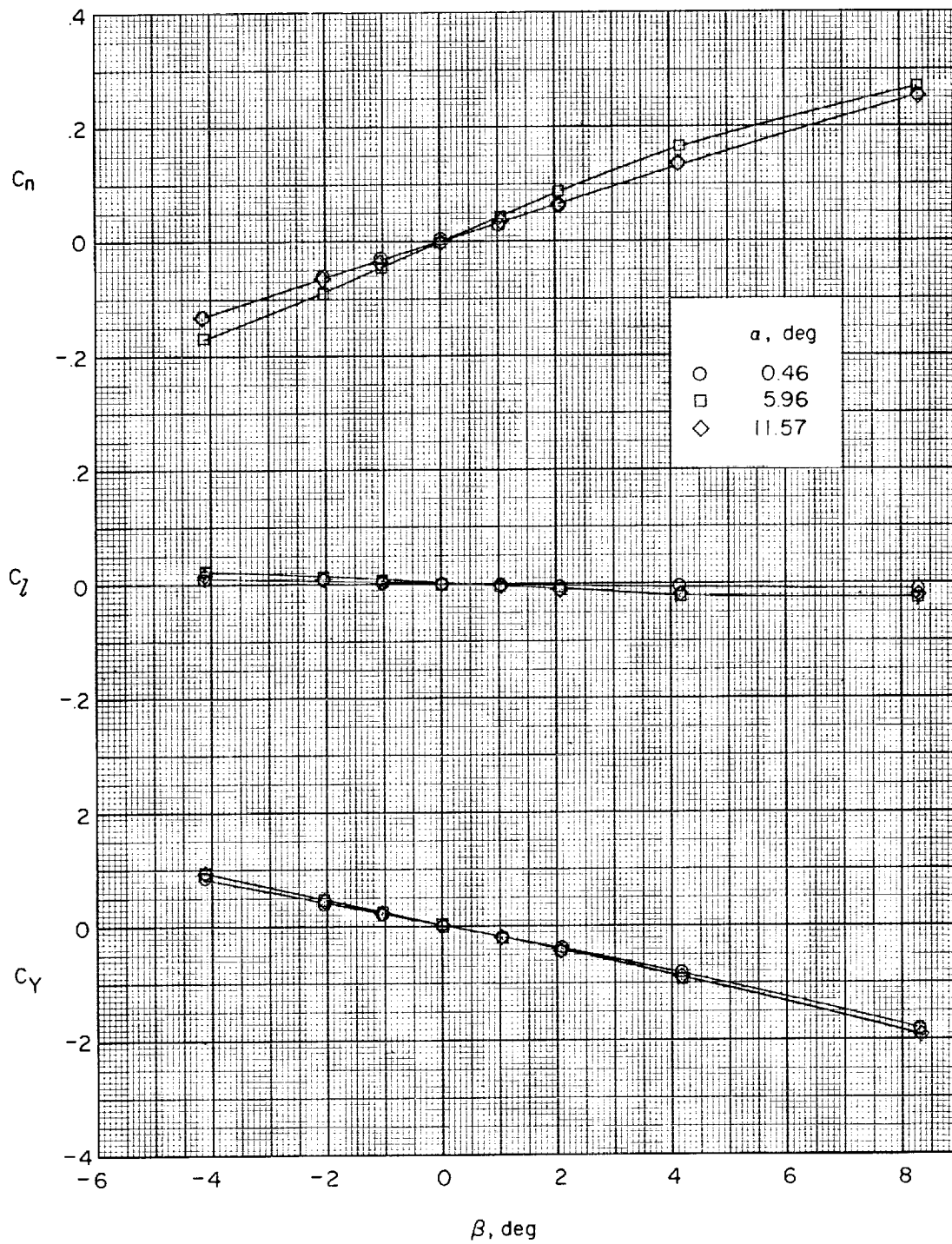
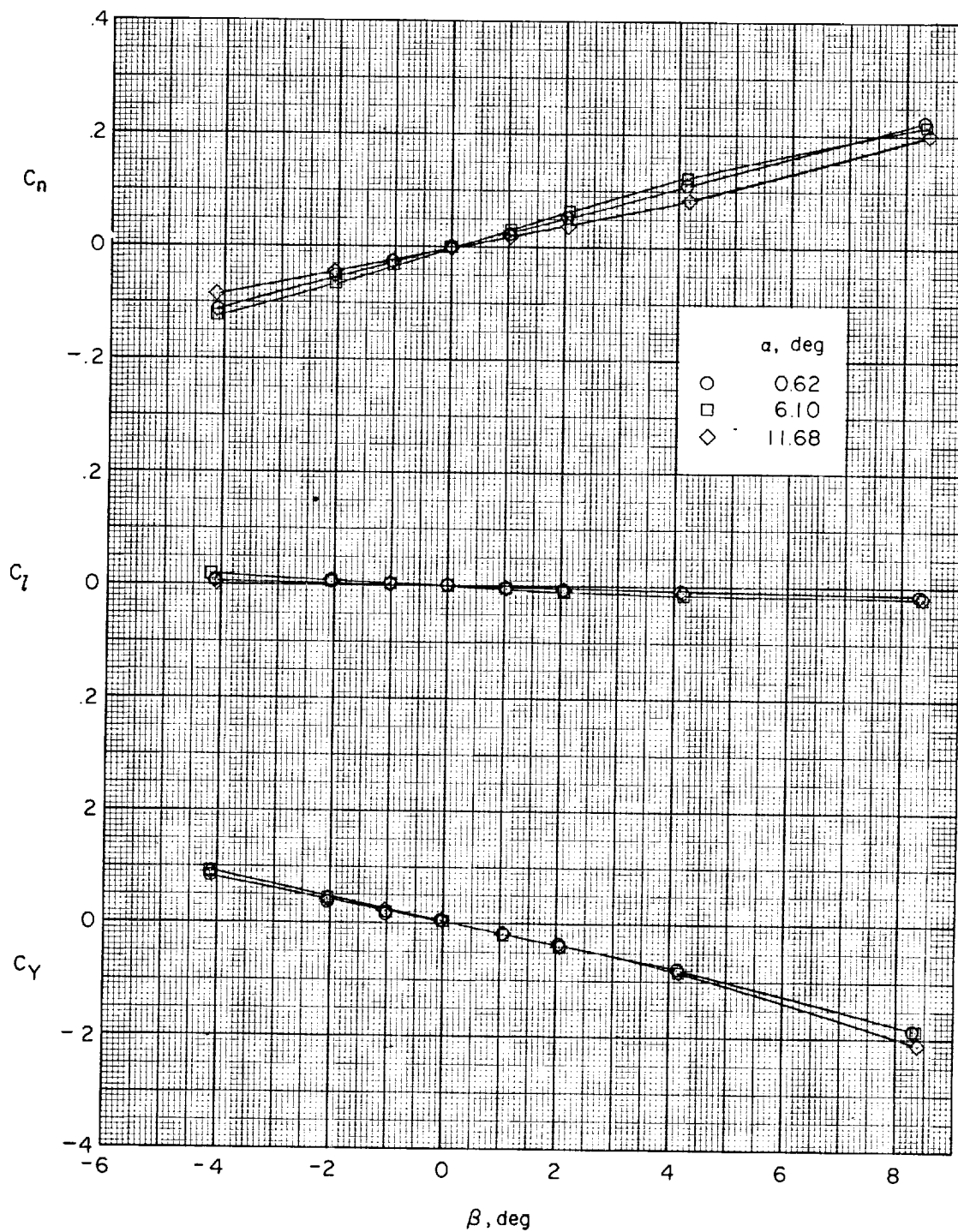


Figure 6.- Summary of longitudinal aerodynamic characteristics of complete model.



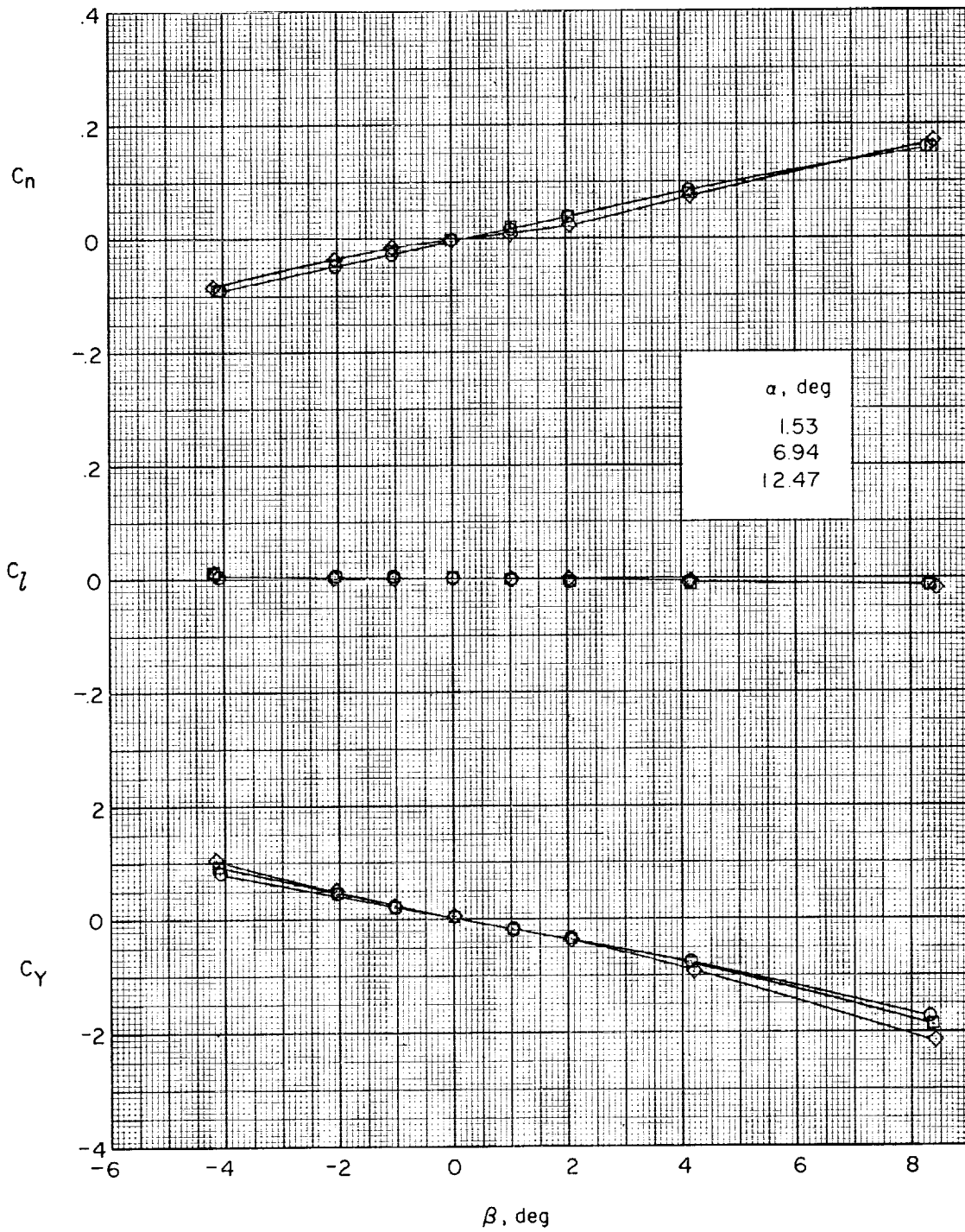
(a)  $M = 1.60$ .

Figure 7.- Effect of angle of attack on lateral aerodynamic characteristics of BWTC.



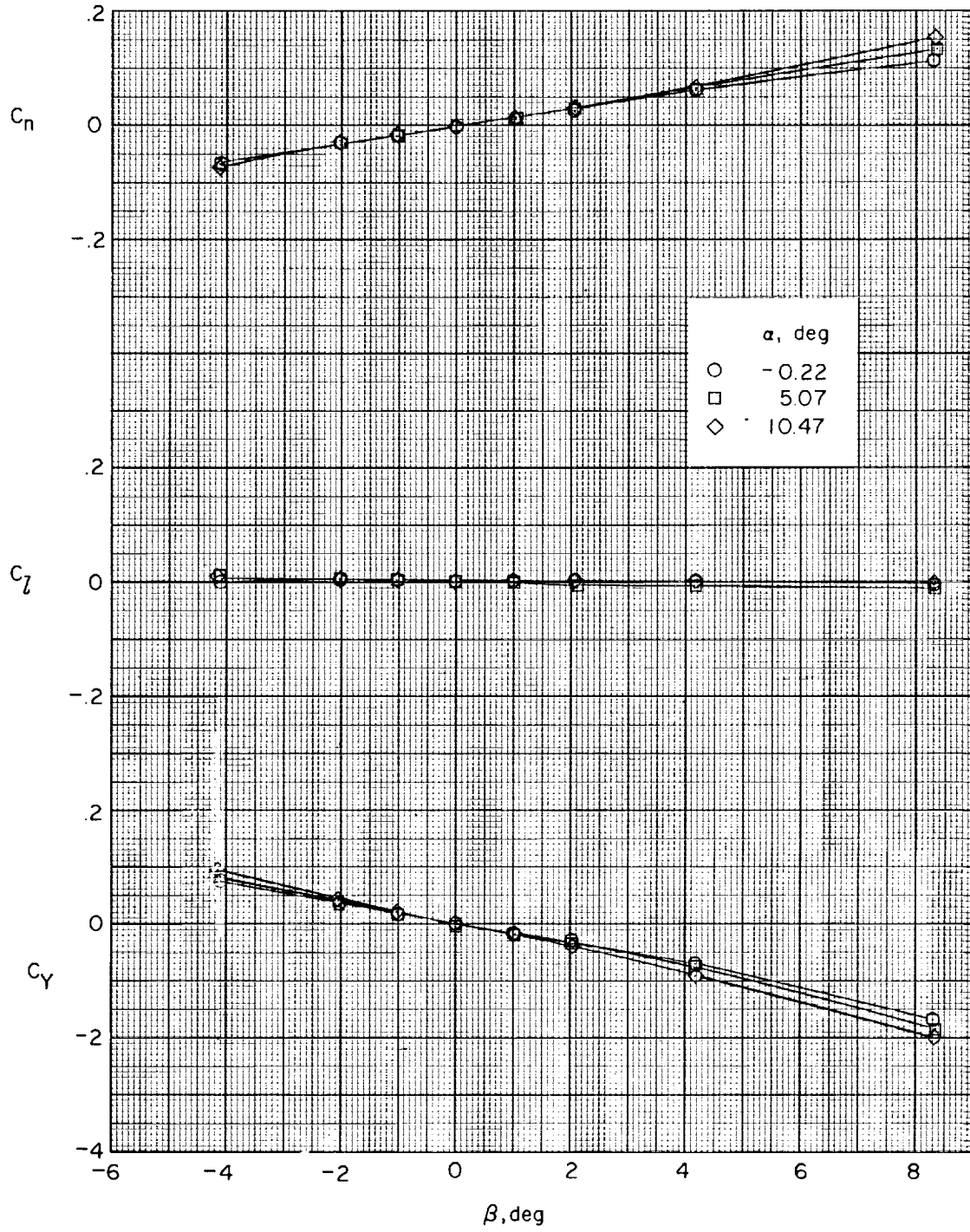
(b)  $M = 1.90$ .

Figure 7.- Continued.



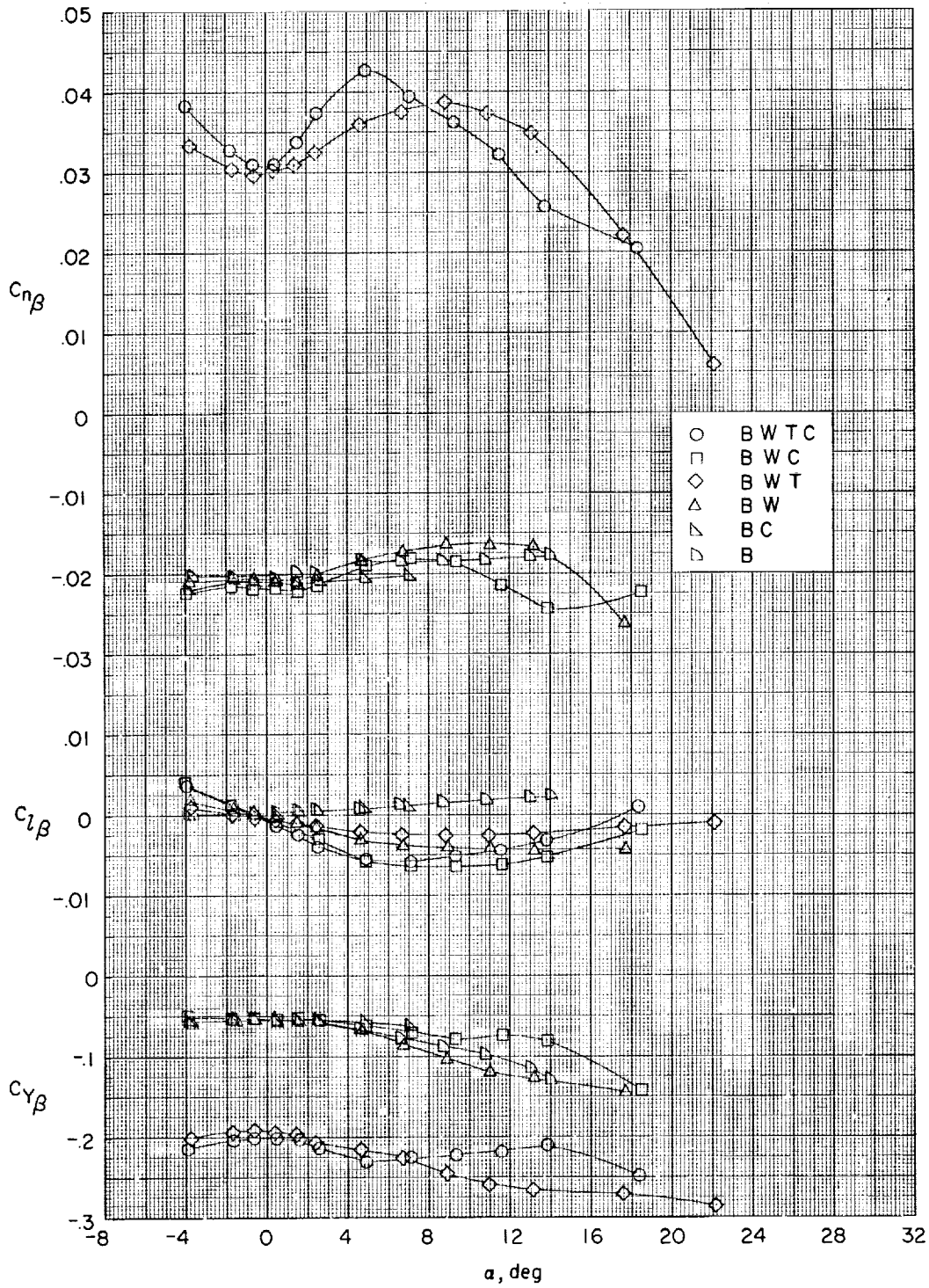
(c)  $M = 2.36$ .

Figure 7.- Continued.



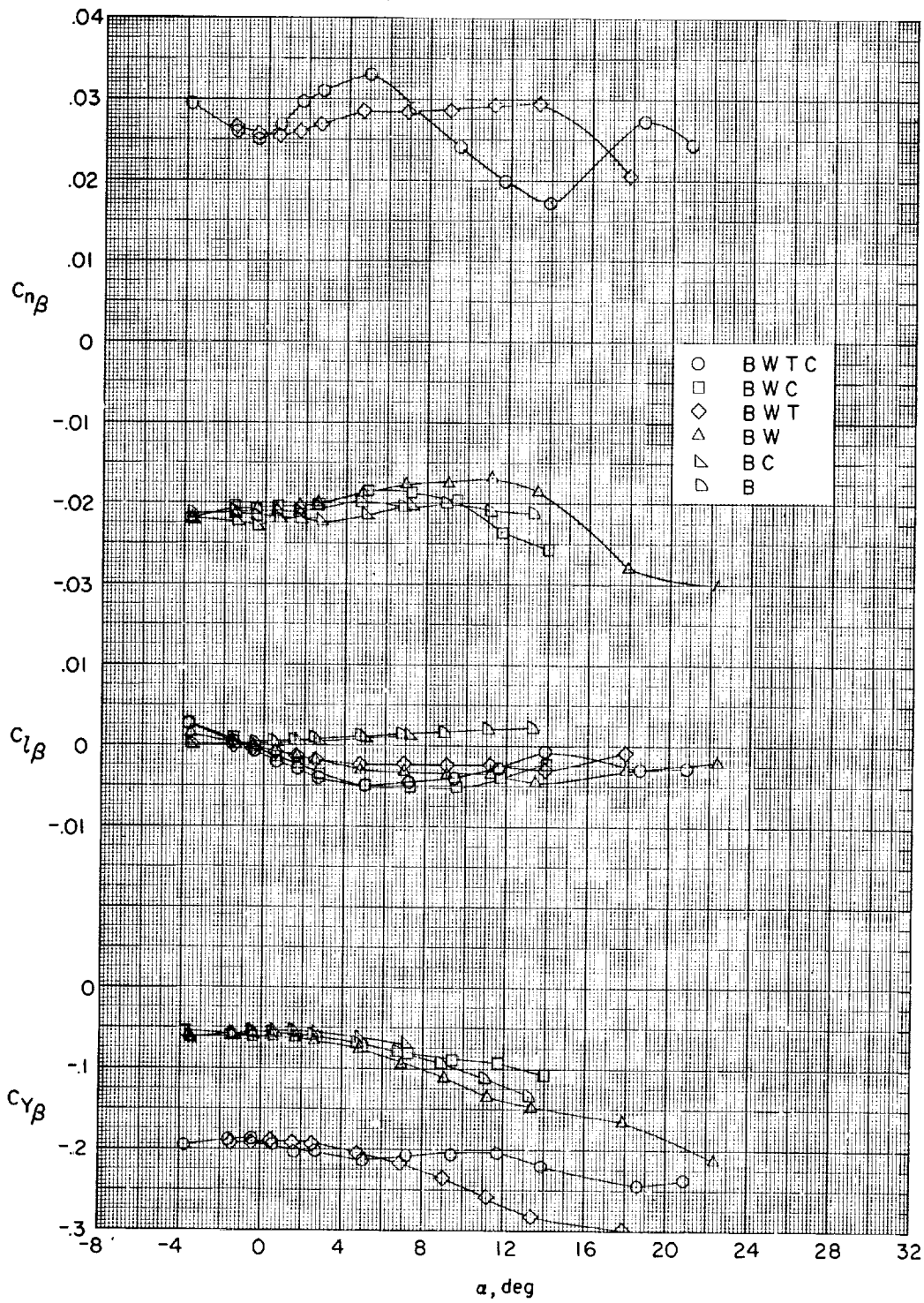
(d)  $M = 2.86$ .

Figure 7.- Concluded.



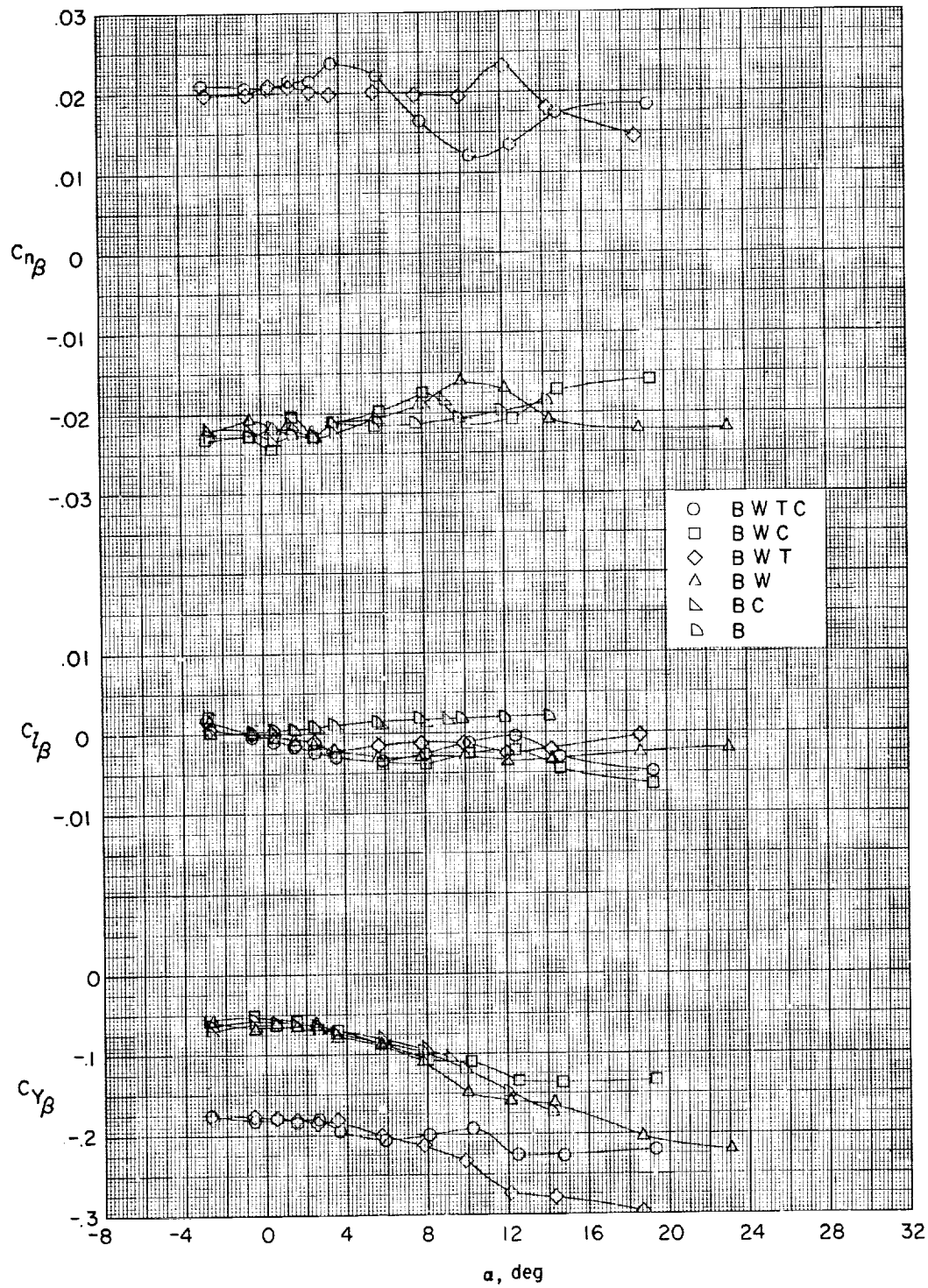
(a)  $M = 1.60$ .

Figure 8.- Lateral derivatives for various model arrangements.



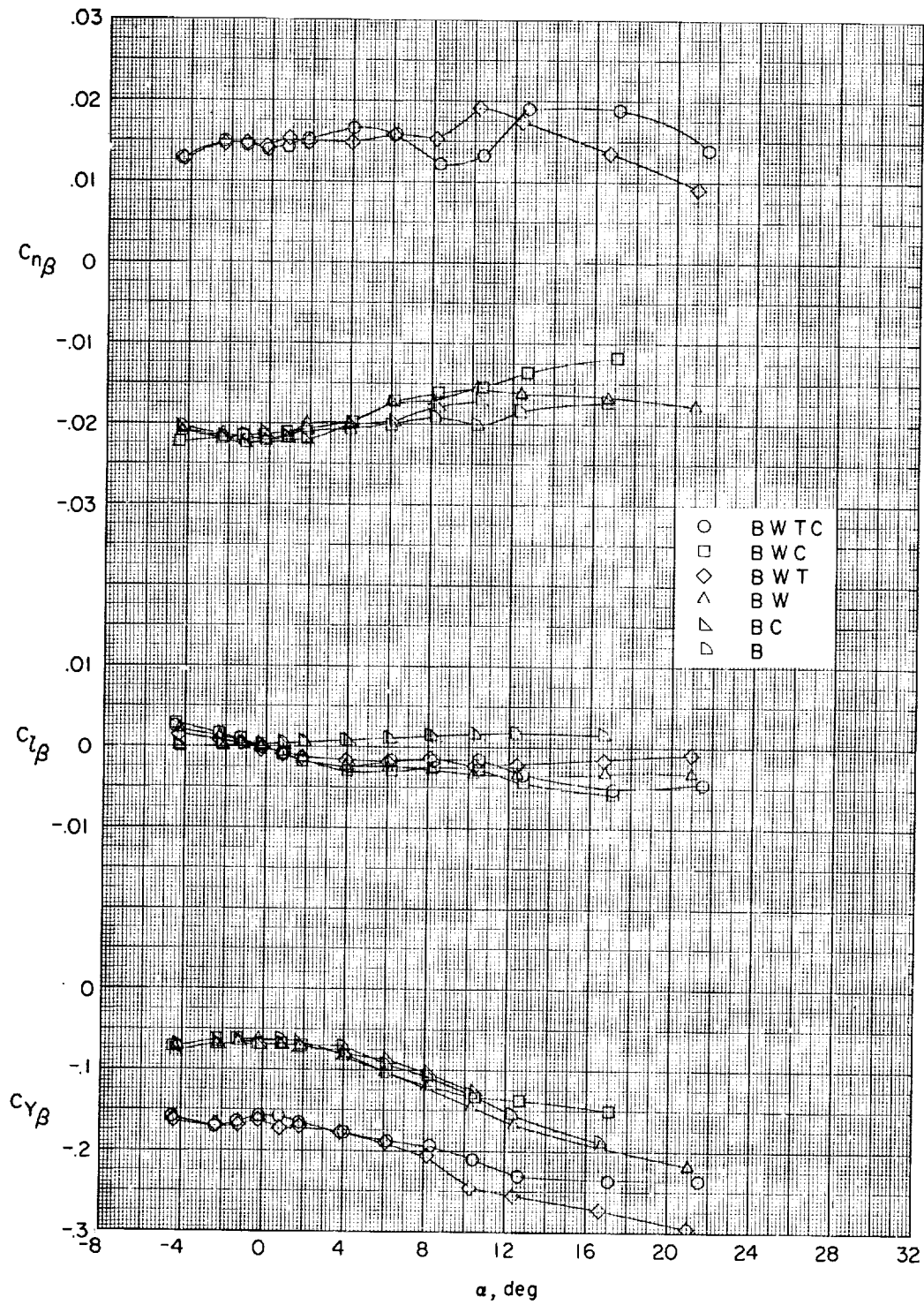
(b) M = 1.90.

Figure 8.- Continued.



(c)  $M = 2.36$ .

Figure 8.- Continued.



(d) M = 2.86.

Figure 8.- Concluded.

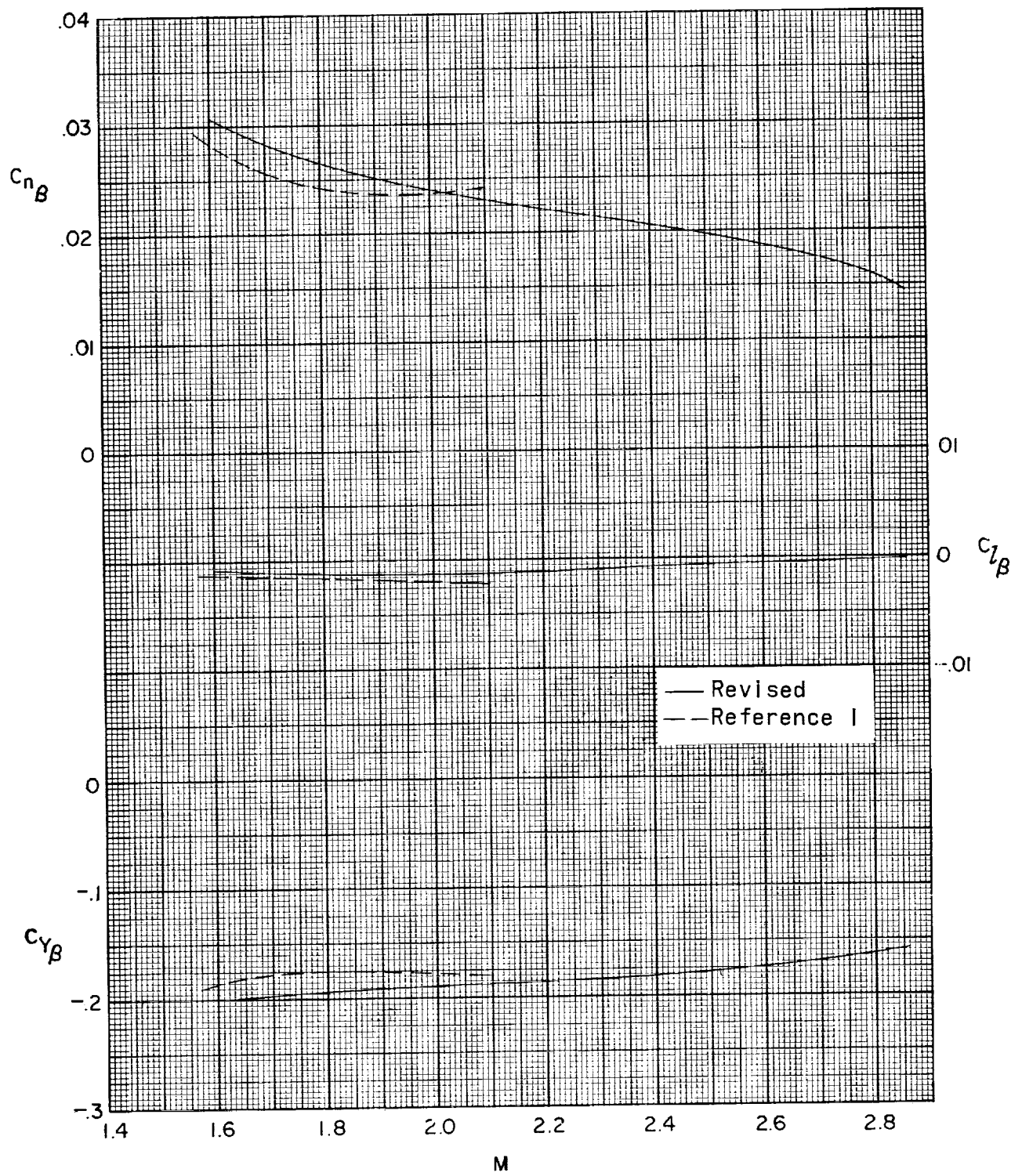
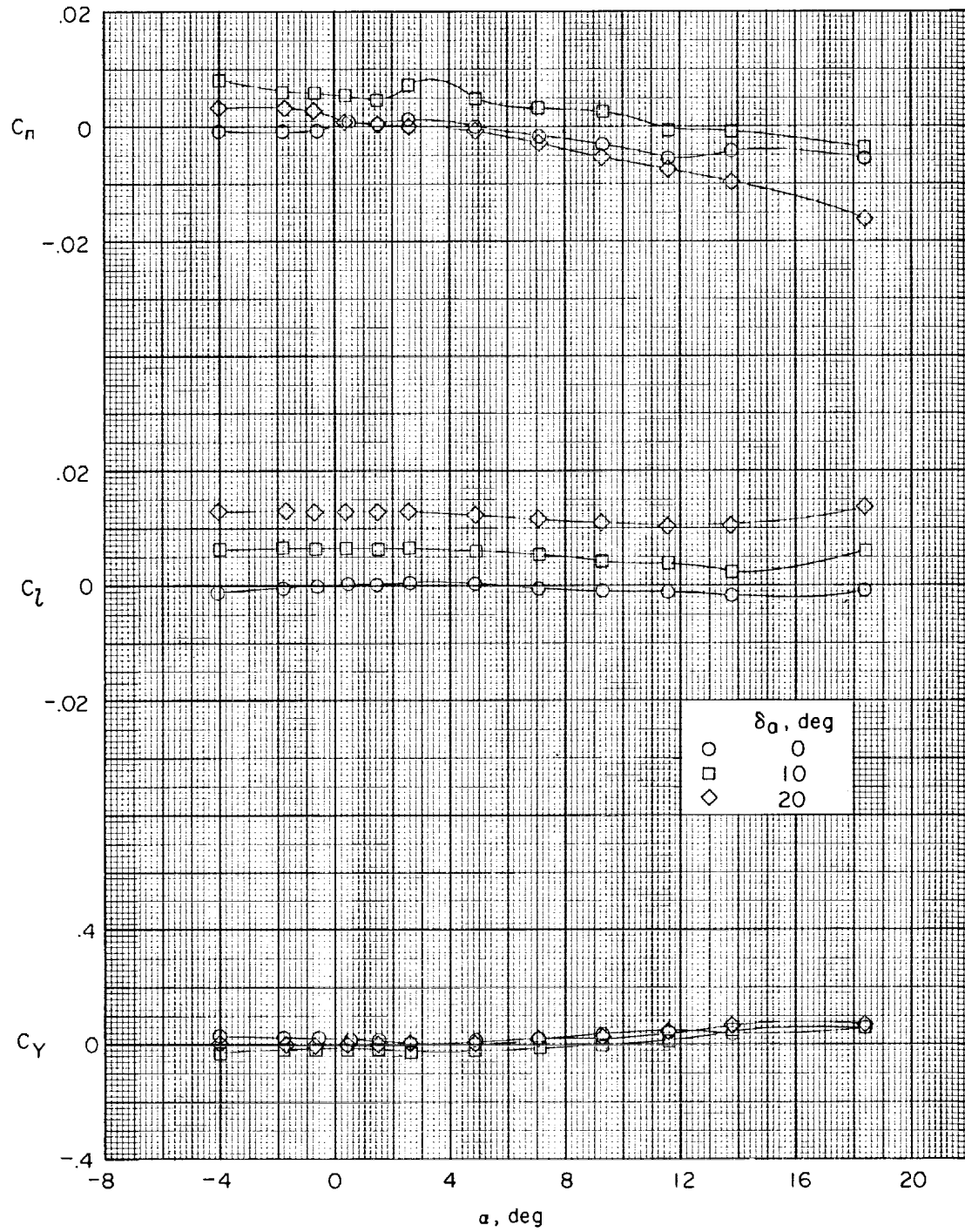
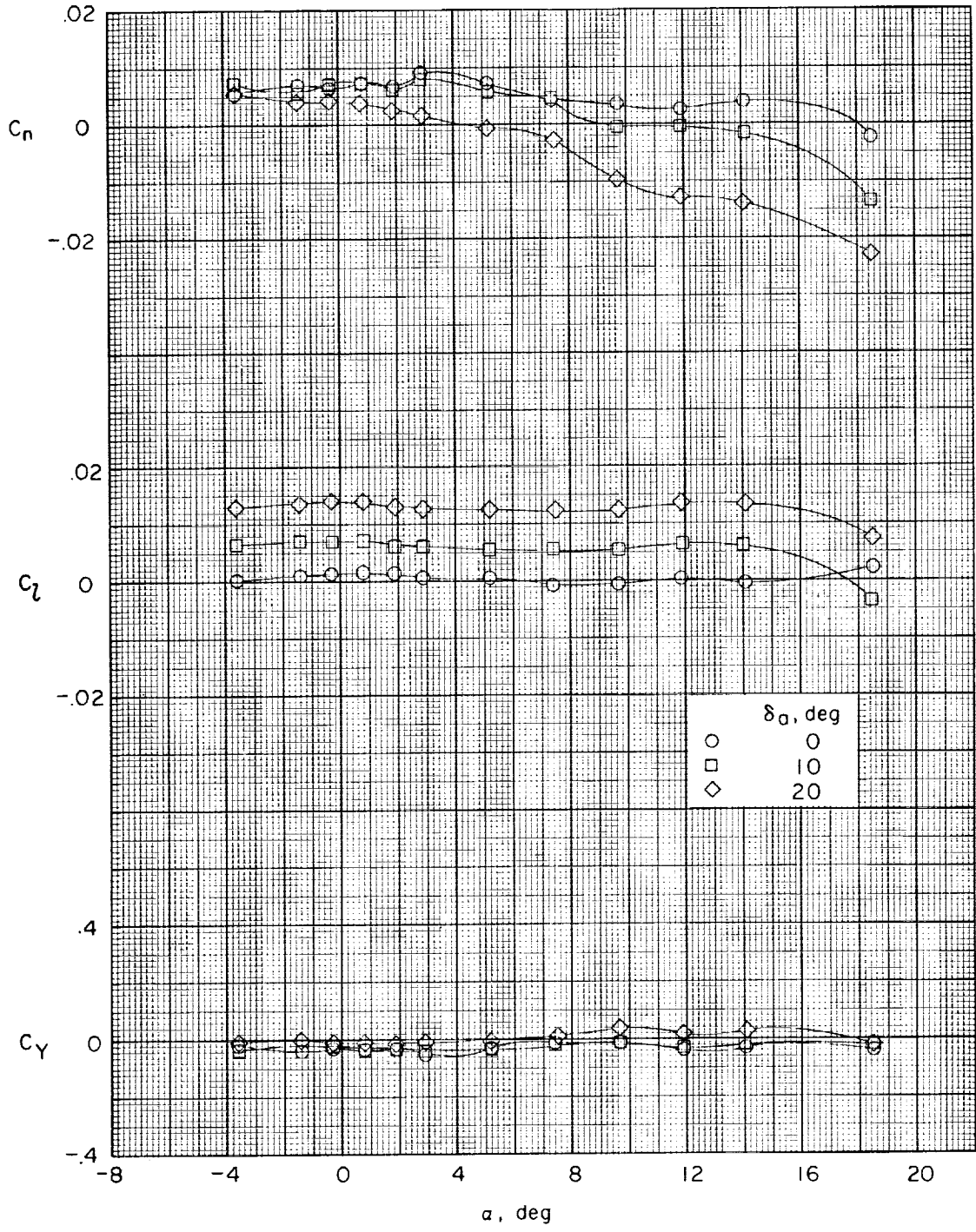


Figure 9.- Summary of lateral and directional stability derivatives of complete model.  $\alpha \approx 0^\circ$ .



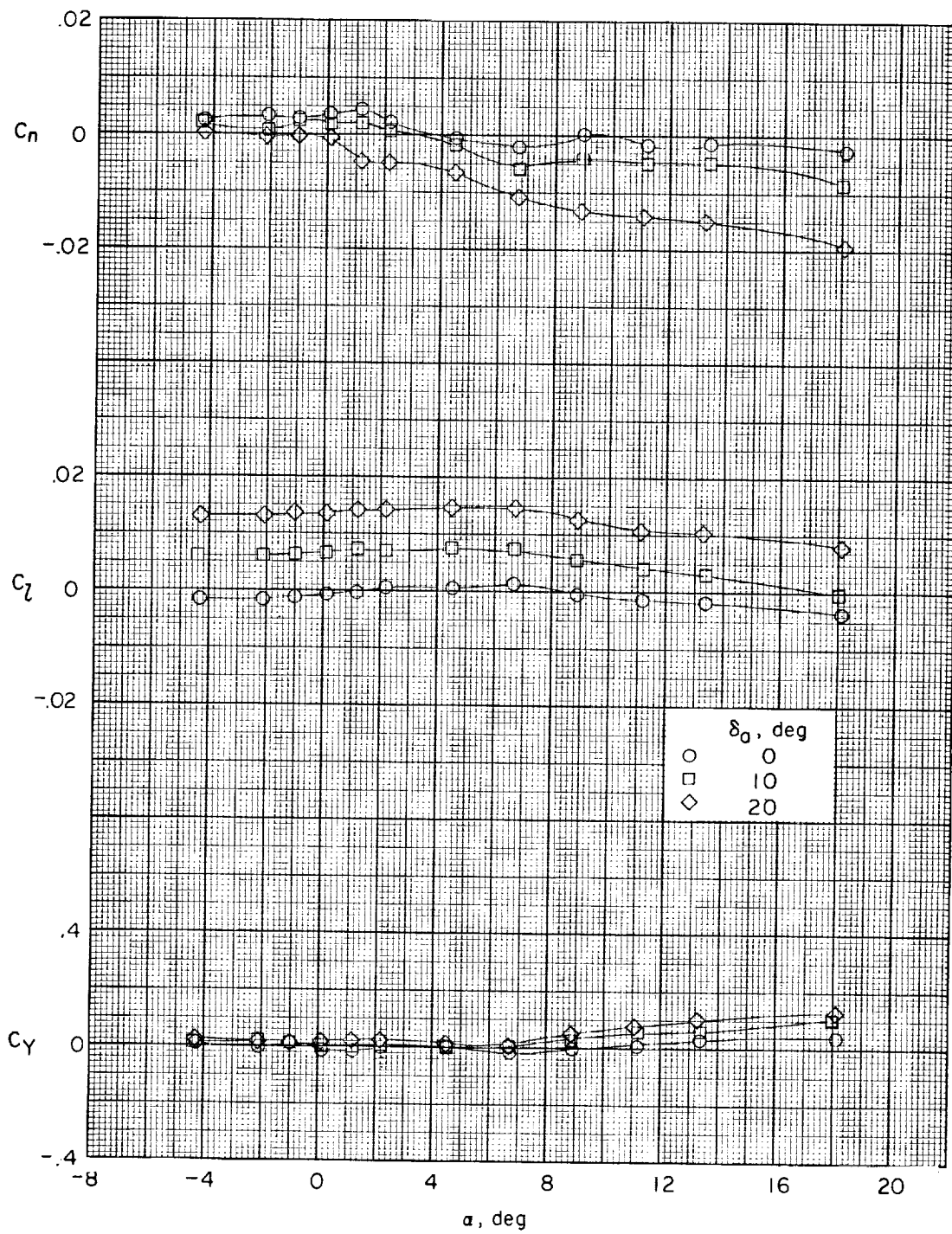
(a)  $M = 1.60$ ;  $\delta_c = 0^\circ$ .

Figure 10.- Aileron-control effectiveness of BWTC.



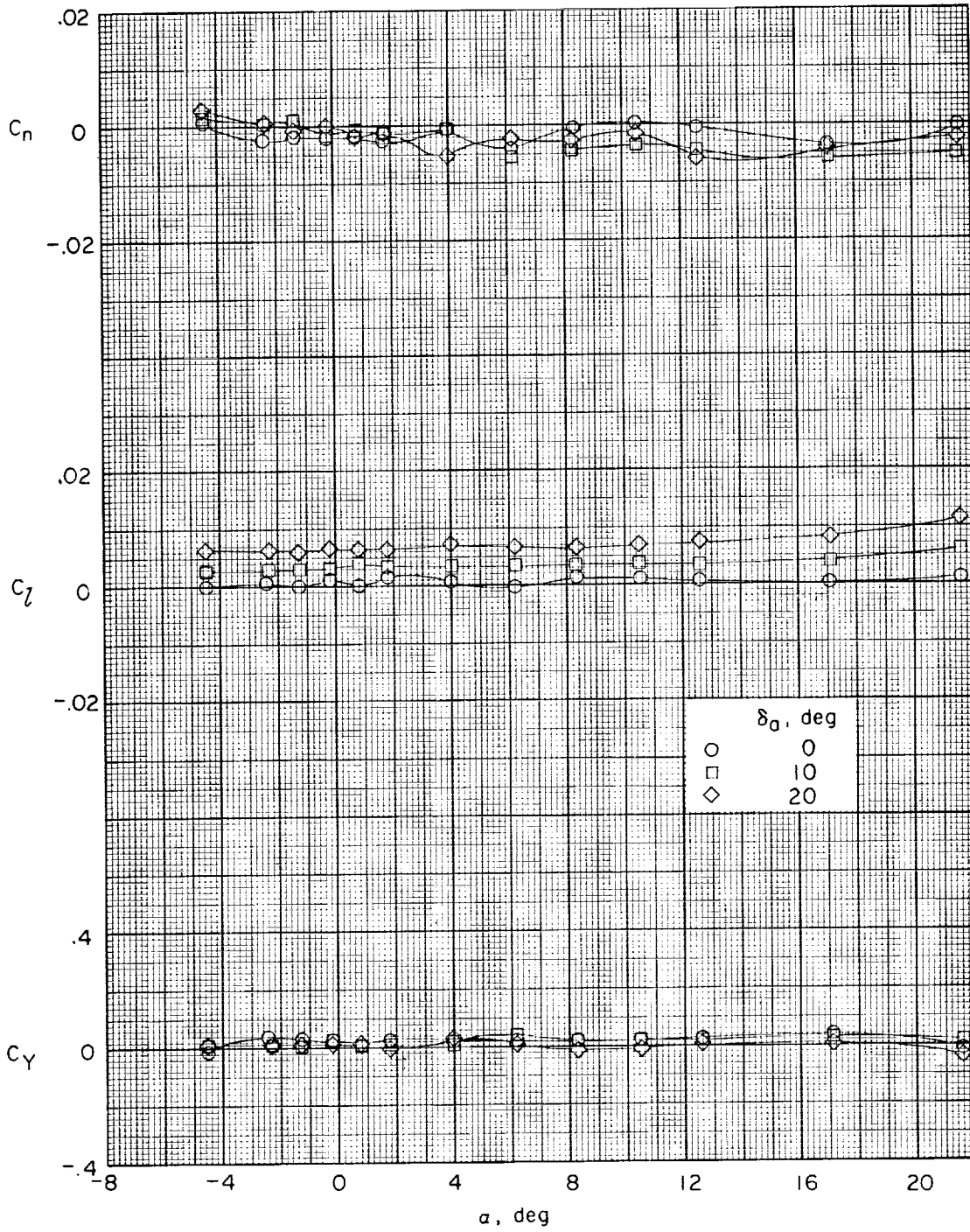
(b)  $M = 1.60$ ;  $\delta_c = 10^\circ$ .

Figure 10.- Continued.



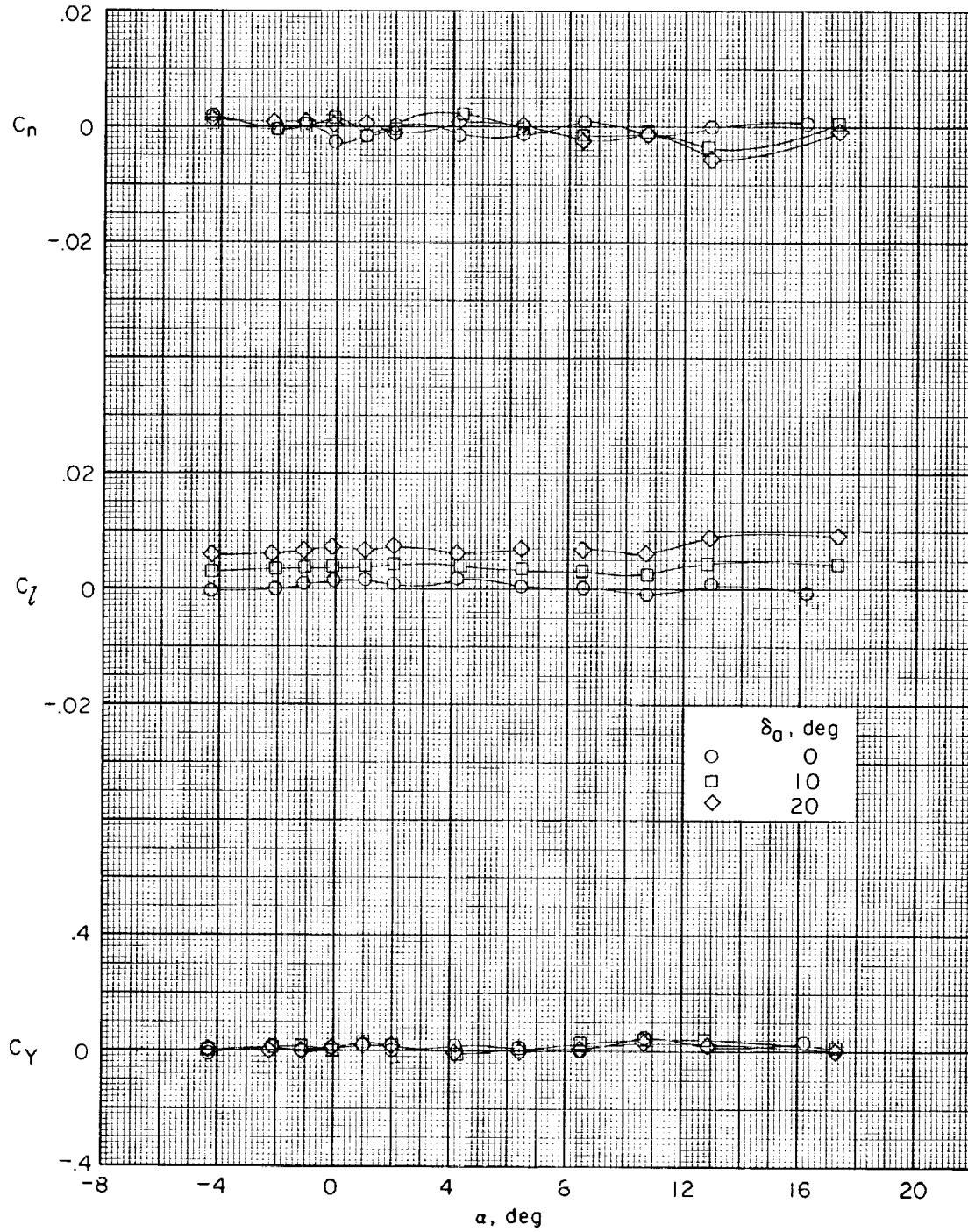
(c)  $M = 1.60$ ;  $\delta_c = -10^\circ$ .

Figure 10.- Continued.



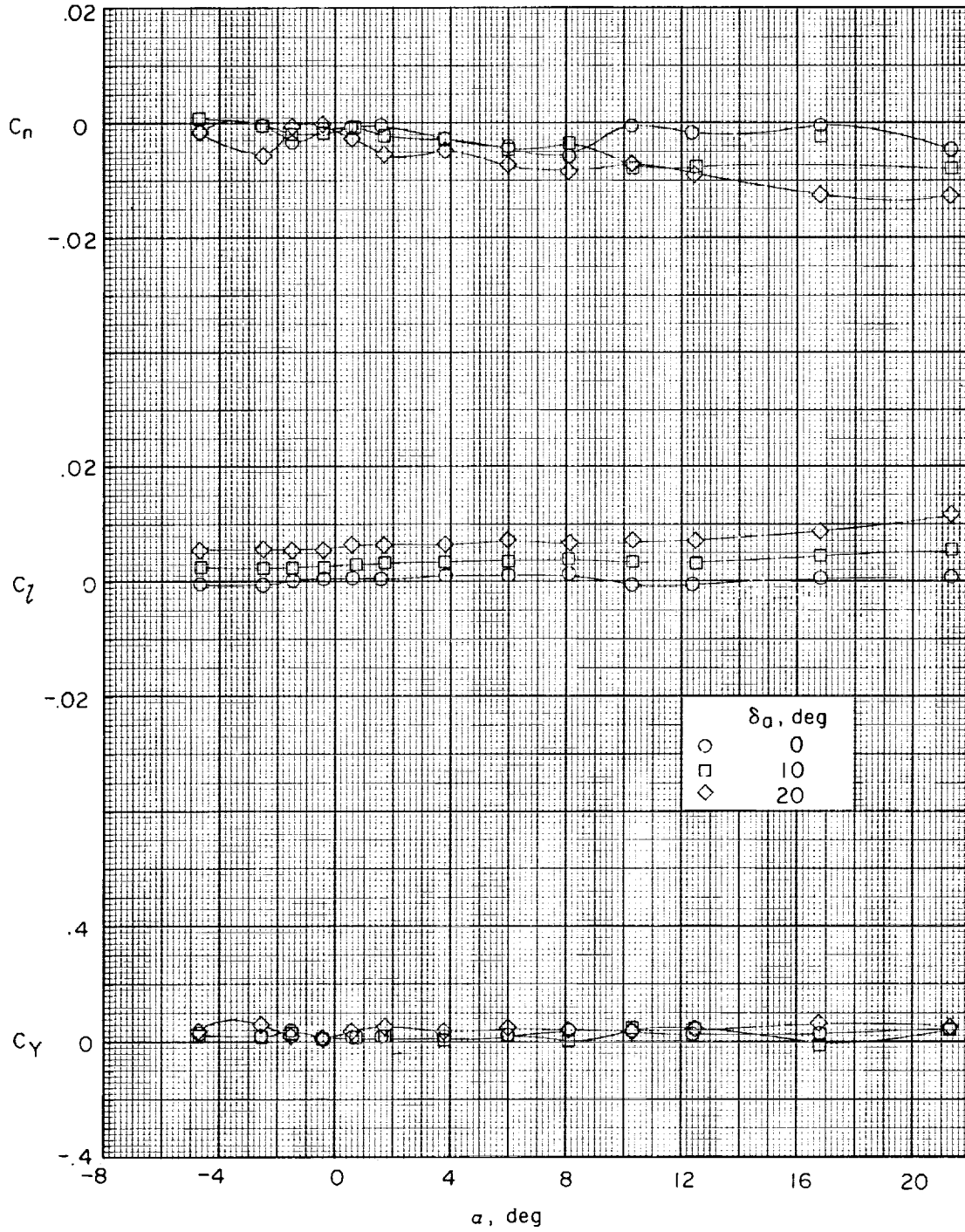
(d)  $M = 2.86$ ;  $\delta_c = 0^\circ$ .

Figure 10.- Continued.



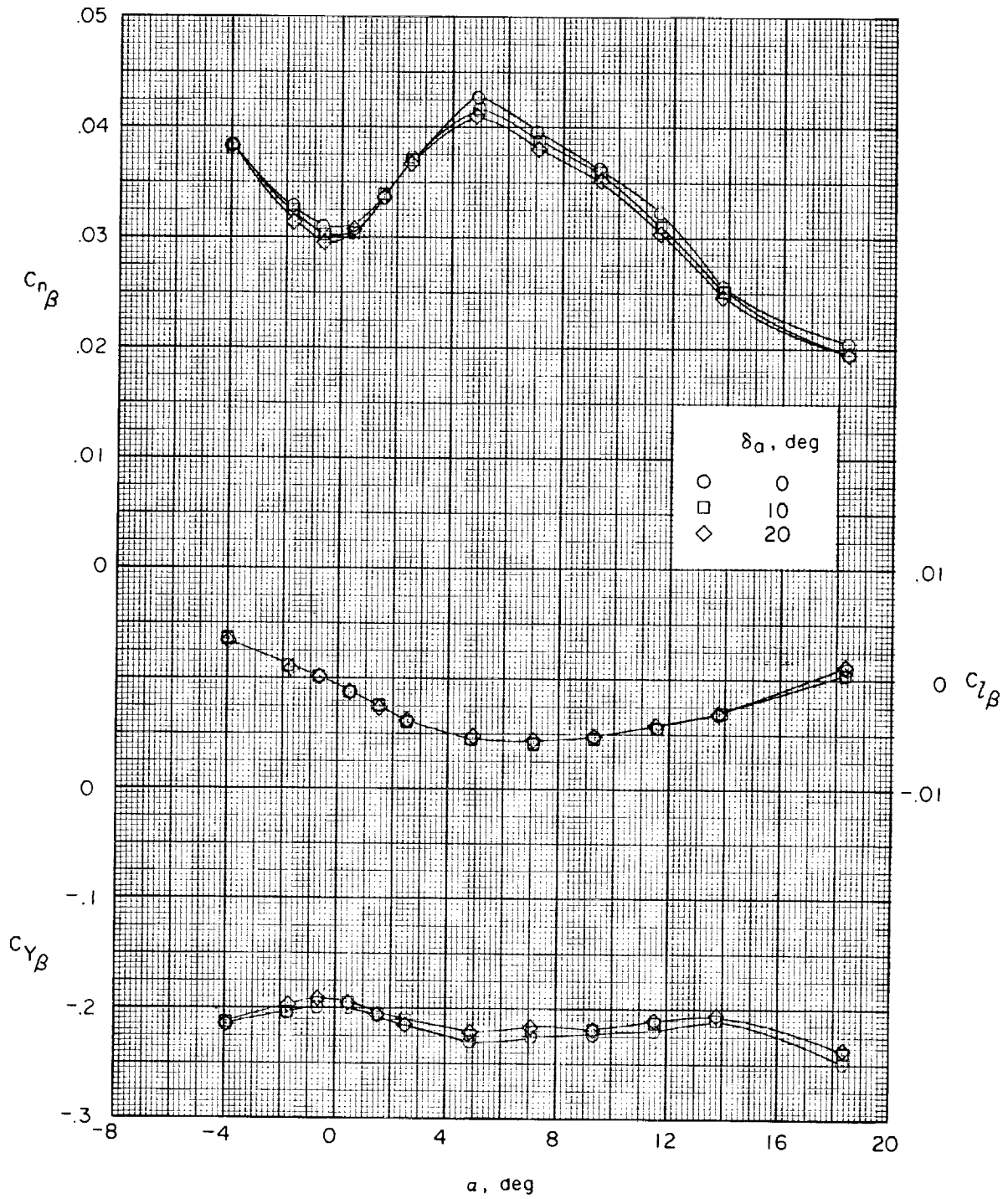
(e)  $M = 2.86$ ;  $\delta_c = 10^\circ$ .

Figure 10.- Continued.



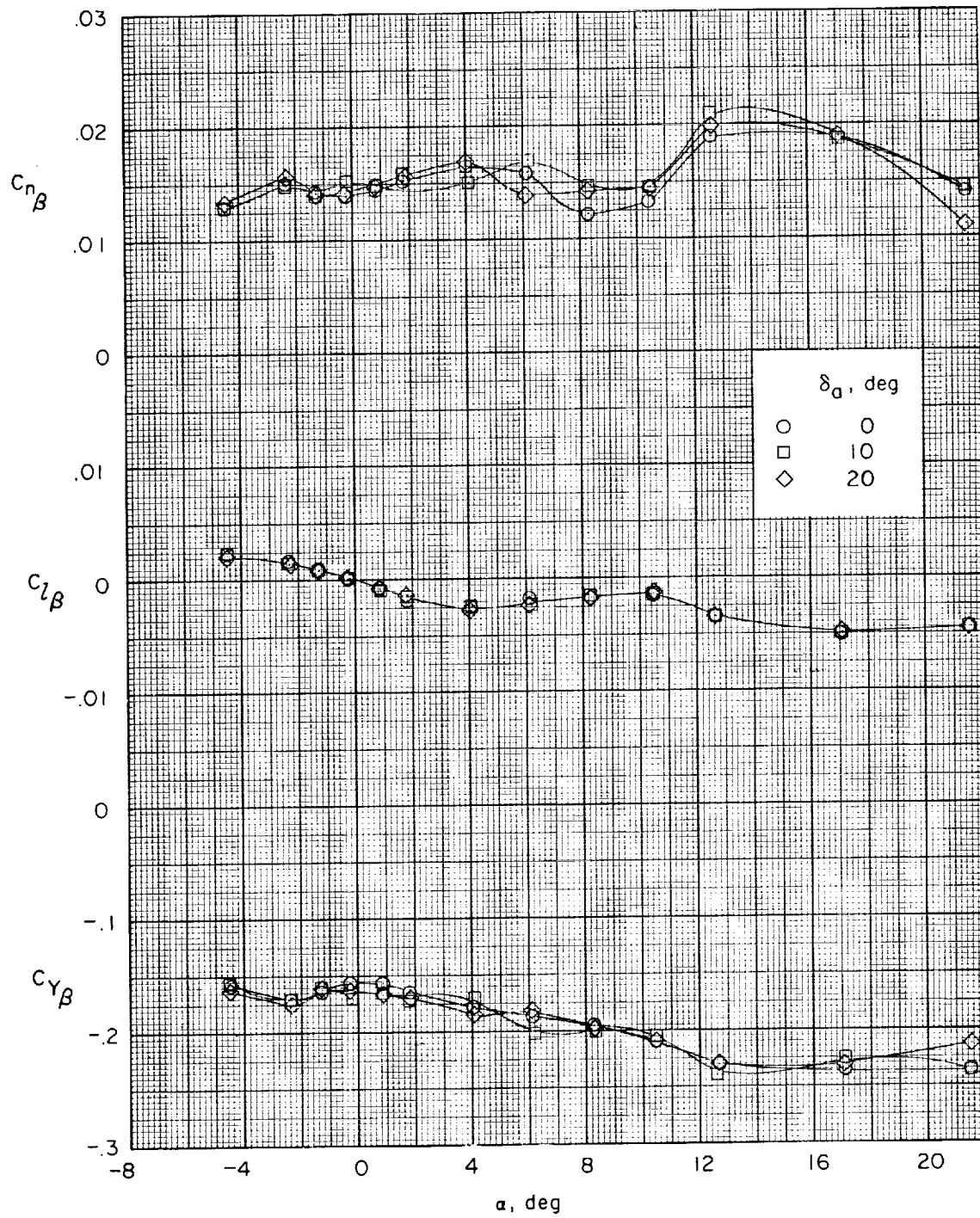
(f)  $M = 2.86$ ;  $\delta_c = -10^\circ$ .

Figure 10.- Concluded.



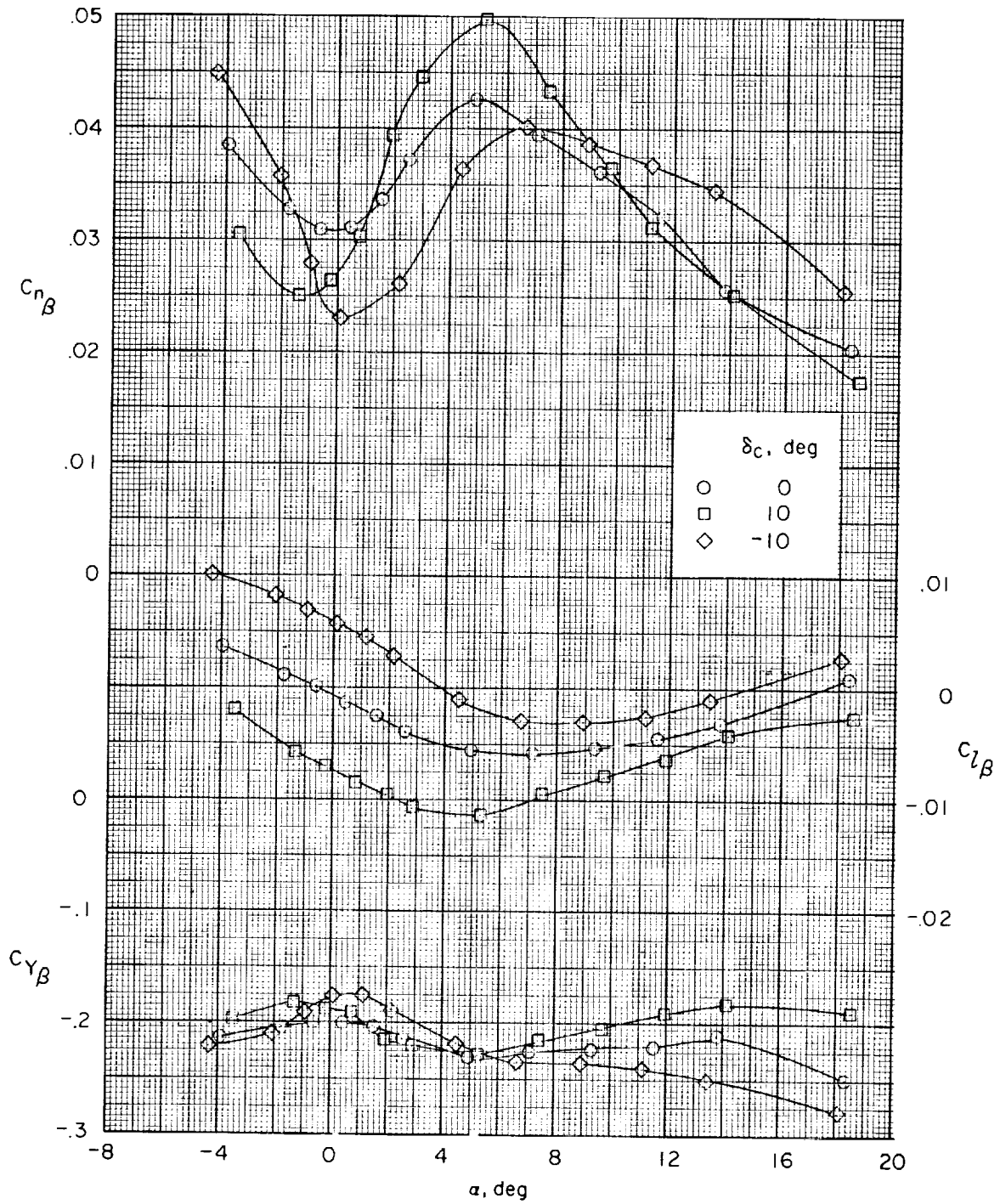
(a) M = 1.60.

Figure 11.- Effect of aileron deflection on lateral stability of BWTC.



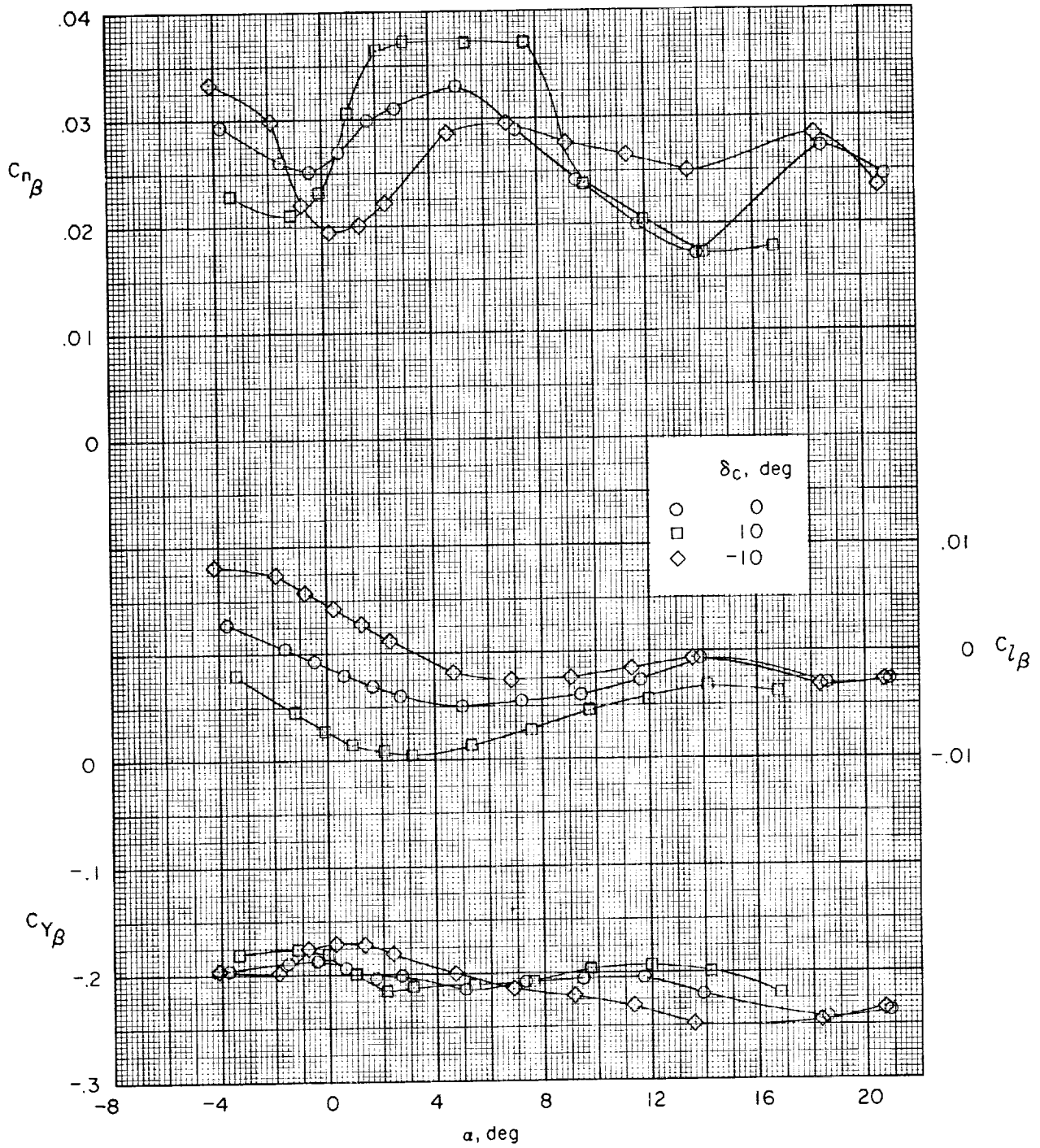
(b)  $M = 2.86$ .

Figure 11.- Concluded.



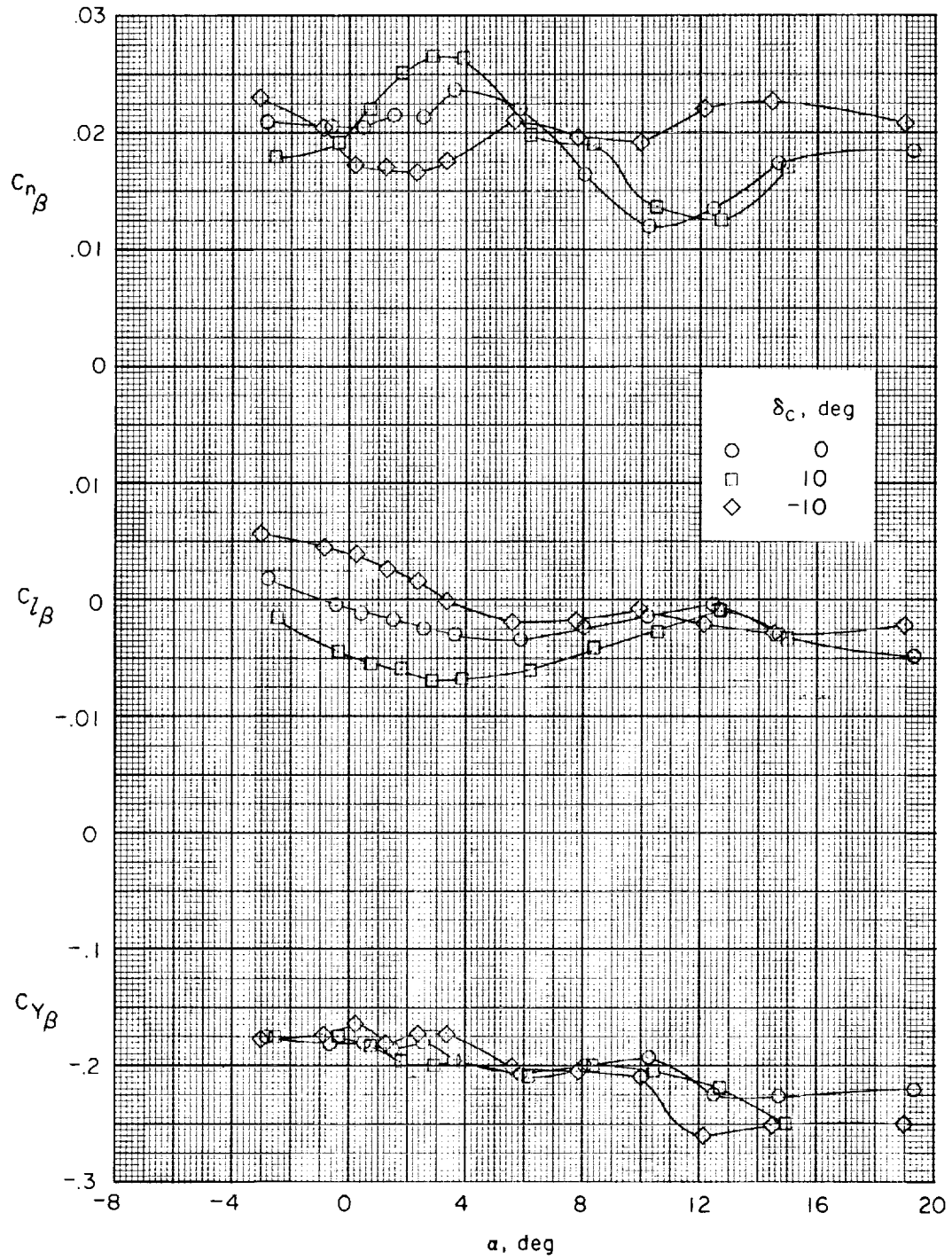
(a)  $M = 1.60$ .

Figure 12.- Effect of canard deflection on lateral stability of BWTC.



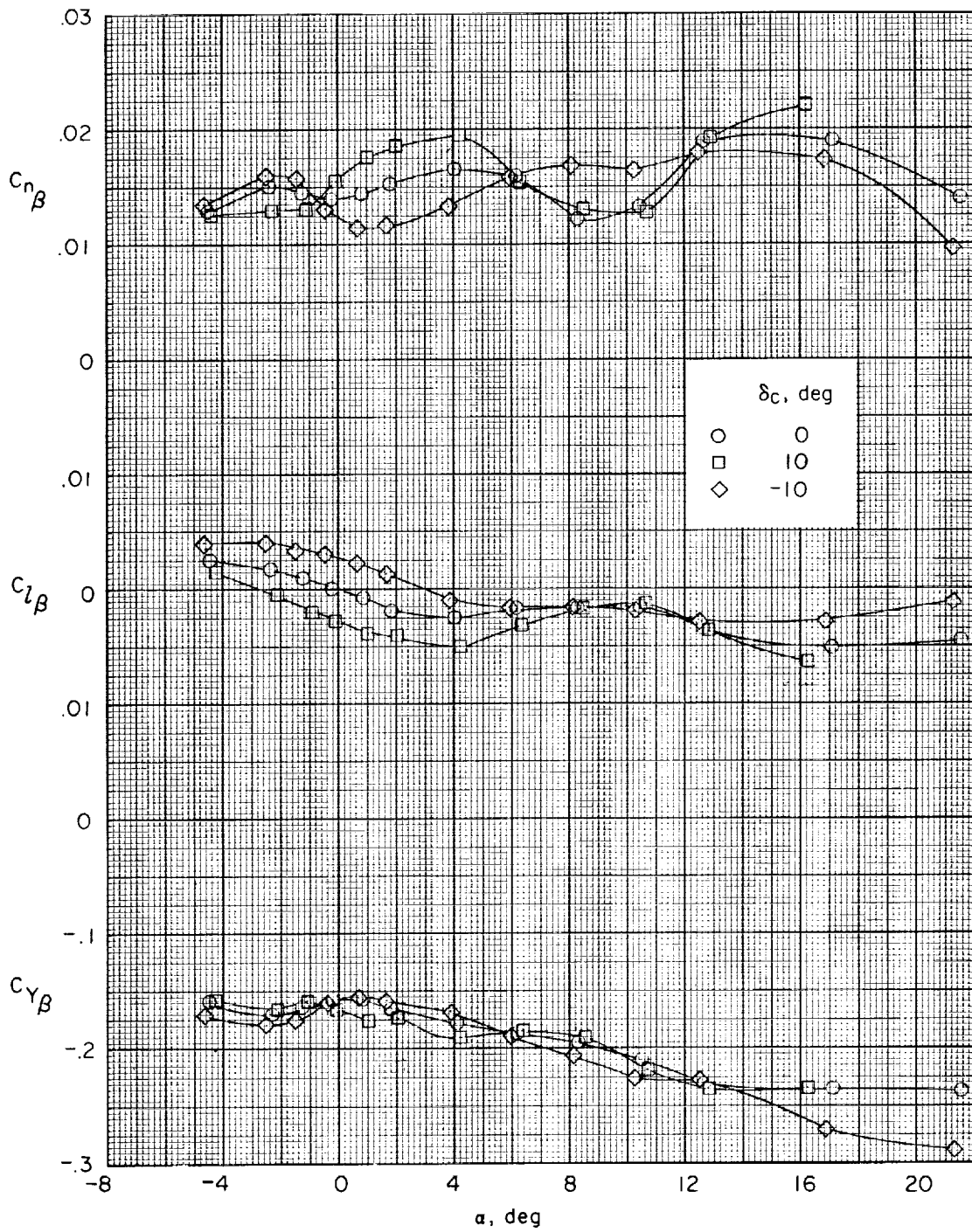
(b)  $M = 1.90$ .

Figure 12.- Continued.



(c)  $M = 2.36$ .

Figure 12.- Continued.



(d)  $M = 2.86$ .

Figure 12.- Concluded.